NEA/NSC/DOC(93)25

Organisation for Economic Cooperation and Development (OECD)

Nuclear Energy Agency (NEA)

Nuclear Science Committee (NSC)

RESULTS OF LWR CORE TRANSIENT BENCHMARKS

H. Finnemann and H. Bauer

Siemens AG - Power Generation Group (KWU)

A. Galati and R. Martinelli

ENEA Casaccia - Advanced Reactor Department

October 1993

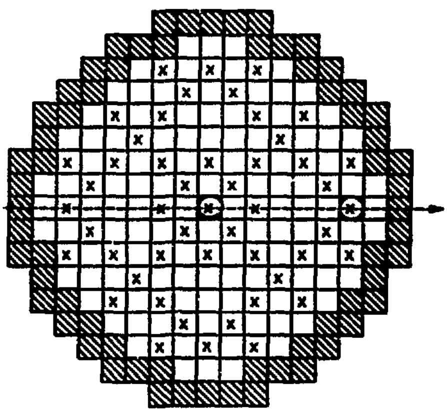

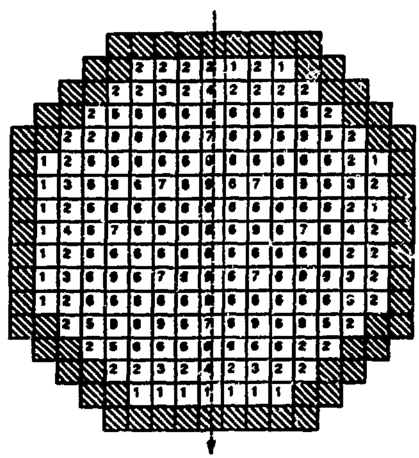

AEN NEA

ORGANISATION FOR ECONOMIC CO-OPERATION AND DEVELOPMENT i+c [?]

NEA/NSC/DOC(93)25

Organisation for Economic Cooperation and Development (OECD)

Nuclear Energy Agency (NEA)

Nuclear Science Committee (NSC)

RESULTS OF
LWR CORE TRANSIENT BENCHMARKS

H. Finnemann and H. Bauer

Siemens AG - Power Generation Group (KWU)

A. Galati and R. Martinelli

ENEA Casaccia - Advanced Reactor Department

October 1993

ORGANISATION FOR ECONOMIC CO-OPERATION AND DEVELOPMENT

RESULTS OF LWR CORE TRANSIENT BENCHMARKS

H. Finnemann and H. Bauer
Siemens AG, Power Generation Group (KWU), D–8520 Erlangen, Germany
Tel. +49(9131) 18–2317, Fax +49(9131) 18–5243

A. Galati and R. Martinelli
Advanced Reactors Department, ENEA Casaccia, Rome, Italy
Tel. +39 (6) 3048–3452, Fax +39 (6) 3048–6478

ABSTRACT

LWR core transient (LWRCT) benchmarks, based on well defined problems with a complete set of input data, are used to assess the discrepancies between three–dimensional space–time kinetics codes in transient calculations.

The PWR problem chosen is the ejection of a control assembly from an initially critical core at hot zero power or at full power, each for three different geometrical configurations. The set of problems offers a variety of reactivity excursions which efficiently test the coupled neutronic/thermal–hydraulic models of the codes. The 63 sets of submitted solutions are analyzed by comparison with a nodal reference solution defined by using a finer spatial and temporal resolution than in standard calculations.

The BWR problems considered are reactivity excursions caused by cold water injection and pressurization events. In the present paper, only the cold water injection event is discussed and evaluated in some detail. Lacking a reference solution the evaluation of the 8 sets of BWR contributions relies on a synthetic comparative discussion.

The results of this first phase of LWRCT benchmark calculations are quite satisfactory, though there remain some unresolved issues. It is therefore concluded that even more challenging problems can be successfully tackled in a suggested second test phase.

Contents page

List of Tables

List of Figures

1 INTRODUCTION

Over the past decade, the Reactor Physics Committee of the Nuclear Energy Agency (NEACRP, now merged into the NEANSC) has been active in promoting or sponsoring several international standard problems on a variety of subjects relating to neutronics aspects of fission reactor operation, core design and fuel cycle analysis.

The subject of the computational benchmark discussed in this paper is the calculation of reactivity transients in commercial-size light water reactor (LWR) cores, via space–time kinetics codes: a timely subject, in the light of the number of such codes which are known to have recently reached a stage of advanced development or a testing phase. The general objective of the benchmark is to carry out a first survey of the state of the art in this area of analysis. Most codes are based on three–dimensional coarse–mesh methods to treat conditions where power distribution changes in space and time cannot safely be assumed to be separable: comparing the performances of such methods – in terms of both modeling and numerics – when coupled with thermal–hydraulics modules is of primary interest in this exercise.

As the evaluation of specific methodologies used to generate the input parameters is outside the scope of the benchmark, all the two–group neutron cross sections and most thermal–hydraulics data are imposed by the specifications document [1] prepared and distributed in 1991 by Siemens AG/KWU (Germany) and ENEA (Italy) who also agreed to coordinate the analysis of the results for the PWR and BWR problems, respectively.

2 PWR PROBLEMS

One of the standard problems of PWR core safety analysis is the rod ejection accident, which may occur as a consequence of the rupture of the drive mechanism housing. This event can produce significant, well localized perturbations of neutronic and thermal–hydraulic core parameters, without exceeding thermal margins. Hence, this realistic problem has been proposed to the participants to efficiently test the neutronic and thermal–hydraulic models of space–time kinetics codes.

The transients are initiated from hot zero power (HZP, 2775 W) and full power states (FP, 2775 MW), for three different configurations each. The cases are denoted by A1, B1, C1 and A2, B2, C2 for the HZP and FP rod ejection transients, respectively. Cases A and B are defined in octant symmetry and further characterized by the ejection of a central (A) or a peripheral (B) control assembly (CA). The PWR benchmark cases are summarized in Tab. 1.

The positions of the CAs are shown on Fig. 1.1 in full core geometry which is used in Cases C1 and C2. As can be seen, the reference PWR core consists of 157 fuel assemblies (FA) and 64 reflector elements. Not shown are the 11 compositions including axial and radial reflector elements which have been specified via macroscopic cross sections and corresponding derivatives [1].

The PWR benchmark participation involved 13 industrial and national institutions from 10 countries. In all 63 data sets have been received and analysed. The submitted solutions are listed in Tab. 2.1 where also the code names and other information on the participants are given. Obviously, cases C1 and C2 were of highest interest for most of the participants. The three cases A, B and C were originally devised to present increasing levels of difficulty for the application of lower dimensional or synthesis models. As can be seen in Tab. 2.2 there are only a few contributions (OKAPI, TRAB, REFLA/TRAC, PRORIA) making use of such approximations. It should also be noted that some of the contributions (e.g. BOREAS, CESAR, COCCINELLE, LWRSIM, SIMTRAN) are based on calculations with a spatial mesh finer than 1 mesh/FA as adopted for the remaining codes. For LWRSIM only a steady-state solution was submitted. OKAPI obtains Doppler effect in each axial node by interpolating Doppler tables, pre-generated in 2-D by distributing temperatures or enthalpy increments according to radial power profile. These two methods are respectively referred as "quasi-static" (s) and "adiabatic" (a) and are correspondingly labeled. Direct time integration techniques are used in most of the codes.

2.1 CHOICE OF REFERENCE SOLUTION

No attempt has been made up to now to obtain spatially and temporally converged reference solutions. However, results of nodal calculations with 2x2 neutronic and thermal hydraulic meshes per assembly are used as references for the purpose of evaluation of the individual solutions. In view of the high spatial accuracy of advanced nodal methods this appears to be an acceptable procedure. Most of the nodal solutions submitted were obtained with one mesh per fuel assembly. The relatively good agreement of these "standard" nodal calculations among themselves and with the reference solution with respect to most of the evaluated parameters indicates that the chosen reference solution well serves its purpose.

Some relevant parameters of the reference calculations performed with PANTHER by P.K. Hutt[2] are given in Tab. 3.1–3.2. Among other neutronic and thermal data the critical boron concentrations and the reactivity worths of the ejected rods are shown . The rod ejection in the HZP cases results in a super prompt critical excursion, as can be derived from the rod worths. The parameters of the final steady-state were found by power searches. Results at the time of power maximum and at the final time t = 5s are also given. As expected, total power and Doppler temperature at the final time are well matched by the results of the power search calculations for the FP cases.

In Tab. 4.1–4.3 sensitivity studies concerning the effect of spatial mesh-size and time step width on reactor power and fuel temperatures are shown. Tab. 4.1 illustrates the small effect of such variations for a rod ejection starting from full power, while the effects are large in case of an initial reactor state at zero power. Tab. 4.2–4.3 indicate that using a finer spatial mesh-size in the PANTHER calculations significantly affects the power peak. On the other hand PANBOX calculations indicate that large changes in the maximum power are also obtained by a smaller time step width. In both, PANTHER and PANBOX studies, the minimum time step is used during the time intervall which covers the power maximum. The final power is almost not affected by those variations. With respect to the fuel temperatures the sensitivity studies clearly show that the main influence is due to the variation of the spatial mesh-size.

2.2 STEADY-STATE RESULTS

The availability of a reference solution highly facilitates the assessment of the discrepancies between the different submitted solutions. The deviation from the reference solution defines a natural quantitative measure of the quality of the evaluated parameters. Obviously, since the temporal evolution of the solution can be strongly dependent on the initial steady-state, the evaluation has to start with the stationary solution. The comparison of the steady-state solutions showed in general a good agreement for local and global parameters. Since in this paper emphasis is placed upon the transient results only a few steady-state parameters can be discussed in more detail, but it may be interesting to note that the maximum power peaking factor is found in the same axial layer and radial position for nearly all the submitted solutions.

Tab. 5.1 shows the deviation of the critical boron concentration from the reference solution. There is quite a good agreement with deviations below about 1 % in most cases except for some non-conforming data in Case A1. This is not easy to understand because the codes concerned performed well in the other HZP calculations. Good agreement with the reference results was also observed for the nodal power peaking factors as can be seen in Tab. 5.2. The somewhat larger deviations of BOREAS, CESAR and LWRSIM in the HZP cases may be partially due to the coarse spatial resolution not quite adequate for the numerical approach used in these codes. A reason for the relatively large deviation of the FP peaking factor calculated by ARROTTA has still to be found. Several participants interpreted the requested power peaking factor as the homogeneous (pin) power peaking factor. It is summarized in Tab. 5.3 and shows rather good agreement among the solutions themselves with the exeption of PRORIA HZP results. The reactivity release due to rod ejection is given in Tab. 5.4.

2.3 TRANSIENT RESULTS

In the following some of the most important parameters of the transient solutions are discussed by comparison with the reference values. The time histories of reactor power and fuel and coolant temperatures in Fig. 2.1 – 7.6 visualize the scatter of data around the reference solution. Deviations shown in Tab. 5.5–5.13 are always to be understood as absolute or relative differences from the reference solution.

2.3.1 REACTOR POWER

Tab. 5.5–5.7 display the deviations of time to power maximum, reactor power peak, and the final reactor power at a time of 5 seconds. Despite the small deviations in the time to power maximum, apart from a few non–conforming data, the power maximum itself shows enormous deviations throughout all HZP cases. As can bee seen in Tab. 5.7, also at the final time some deviations remain very high.

Apart from the TRAB 1–D result the highest positive deviations in the HZP cases are produced by QUABOX–CUBBOX. Though every effort was made, the origin of this discrepancy could not be pinpointed up to now. Other solutions (CESAR, COCCINELLE, PRORIA) exhibit relatively large negative deviations. The OKAPI 1–D adiabatic method shows high positive deviations of the reactor power in contrast to the large negative deviations obtained with the quasi–static approach. The quasi–static model becomes more accurate after a few seconds, when the temperature peak occurs, compared to the adiabatic model which is only suitable for the first fast part of the transient.

The results for the power maximum in the HZP cases seem indeed very sensitive with respect to the computational strategy. This can also be seen in Tab. 5.6 for the solutions obtained with PANBOX, QUANDRY-EN, SIMTRAN, ARROTTA and PANTHER which often form a cluster with the reference solution as indicated in the time histories figures. This fact might not be too surprising considering the similarity of the numerical approach of the codes.

From Fig. 2.2, 4.2, and 6.2 it can be concluded that case B1 seems to be the HZP case producing best agreement among the power histories by forming a cluster existing of OKAPI (s), TRAB, PANBOX, QUANDRY, SIMTRAN, and PANTHER results, whereas in case C1 only PANBOX, QUANDRY-EN, SIMTRAN, and PANTHER show similar results. Surprisingly, since the well symmetrical case A1 has been expected to be the most easiest case to calculate, no formation of a well defined cluster can be seen at all (Fig. 2.2).

The variation of results in the FP cases is less evident as can also be seen in Tab. 5.5–5.7. A glance at Fig. 3.2, 5.2, and 7.2 visualizes the dispersion of FP results more clearly. Throughout all FP cases the highest power peaks are obtained with COCCINELLE and QUABOX–CUBBOX and the lowest power peaks and time histories with the OKAPI 1–D static method. On the whole, the agreement of the solutions among themselves and with the reference solution is acceptable. Again, some solutions cluster around the reference solution.

The final steady–state power obtained from power–search calculations is shown in Tab. 5.8 for a few participants only.

2.3.2 POWER DISTRIBUTION

At time of power maximum the deviation of the horizontal traverse elements (see Fig. 1a) of the radial power distribution in axial layer 13 for the full core cases is shown in Tab. 5.12–5.13 (results not available for all codes). The radial power distribution is normalized to the maximum value in this axial layer. With only a few exceptions the maximum node power in Case C1 is found at the position of the ejected CA and in Case C2 in the node on the left of the ejected CA.

2.3.3 FUEL AND COOLANT TEMPERATURES

The deviations of final Doppler, fuel centerline, and coolant outlet temperatures are shown in Tab. 5.9–5.11. The Doppler temperature is a weighted average of the fuel centerline and fuel surface temperature [1]. Since reference 1 was ambiguous in this point, some of the data quoted in Tab. 13 as core averaged Doppler temperature may in fact be volume averages. This would account for some of the larger deviations.

Thus, excluding the TRAB 1–D result, only the low core average Doppler temperature of ARROTTA is noticeable. Most of the other deviations remain below 2 %.

This is also true for the final coolant outlet temperature shown in Tab. 5.11. The results for the final maximum fuel centerline temperature in Tab. 5.10 are also very satisfactory.

Thus the time histories of the <u>core averaged Doppler and maximum nodal fuel centerline temperatures of the HZP cases</u> form a cluster around the reference solution. The fuel temperatures in general follow the time histories of the reactor power, i.e. significant deviations from the reference power (see also tables 5.6–5.7) produce significant different fuel temperature time histories (TRAB–1D, OKAPI 1–D adiabatic). A puzzling fact is the good agreement of fuel temperatures calculated with CESAR, COCCINELLE, and SIMTRAN, though the power histories show large deviations from the reference solution. Similar to the fuel temperatures, the time histories of the <u>coolant exit temperature</u> depend on the transient behaviour of the reactor power. Noticeable are the low coolant temperatures obtained with QUANDRY–EN despite the good agreement in power and fuel temperatures.

With respect to the <u>FP cases</u>, the time histories of Doppler temperature show a rather constant spread of data of about 50 °C, whereas the maximum nodal fuel centerline temperature data spread about 25 °C in case A2 and B2 and 100 °C in case C2. Within the time histories shown, the coolant exit temperature data show a maximum deviation of about 0.5 °C from the reference solution.

Since a few participants interpreted the maximum fuel temperature as the node averaged maximum value, the time histories of this <u>maximum nodal fuel temperature</u> are added to the figures (though no reference solution available).

3 <u>BWR PROBLEMS</u>

Cold water injection and core pressurization transients – the test problems proposed to the participants as Cases D1 and E1, respectively – rank very high in the short list of events for which BWR designers and analysts currently use three–dimensional dynamics. This section reviews the results contributed for Case D1, that attracted wider participation. The BWR benchmark participation involved 8 industrial and national institutions from 5 countries as shown in Tab. 6. The cold water injection over the whole core at the inital power of 1600 MW is simulated by doubling the inlet water subcooling through an exponential increase with a 2.5 s time constant. The reference BWR core consists of 185 fuel and 64 reflector macroelements, each corresponding to four regular subassemblies neutronically homogenized with the pertinent control blade. Nine different fuel macroelement compositions are considered, as shown in Fig. 1.2. Prior to intercomparing the eight 3-D solutions, it may be worth recalling that the specifications, while imposing most parameters, allowed the participants to choose the clad-coolant heat transfer models and the correlations closing the conservation equations in the coolant.

3.1 STEADY-STATE RESULTS

In the following, a synthetic comparative analyses is given of some key parameters calculated at steady-state, from which clues are derived for the interpretation of the transient performance of the codes. In the case of k-eff results, the accuracy of steady-state calculations directly affects the evolution of the transient; in fact, in order to simulate criticality at the transient onset, it is required to divide the average number of neutrons produces per fission by the steady-state eigenvalue.

3.1.1 K-EFFECTIVE

The k-eff results are compared in Table 6. It can be seen that six values are well clustered around the mean (.9859) with deviations below 600 pcm; on the other hand ARROTTA and QUANDRY-EN deviate considerably on opposite sides. There are strong inferences that such discrepancies can be attributed to a large extent to some differences in thermal-hydraulics (rather than neutronics) modeling.
The ARROTTA code has no provisions for calculating pressure drops. As a consequence, a guess must be made of the flow-rate distribution in the core. The (sensible) contributor's choice of a uniform flow-rate, produces an easy-to-check distortion of the void distribution (the hotter the channel, the larger the underestimate of the voids) which ultimately leads to overestimate the k-eff. A more accurate assessment of the reactivity effects due to flatter void (and power) distributions, can confirm the coherence of this assumption with the observed calculational discrepancies.

The low k-eff calculated by QUANDRY-EN can be associated to the slip correlation (slip ratio = 1) adopted in the void model, which produces a systematic overestimate of the void fractions. In fact, by intercomparing the results for a number of outlet variables, it is easily shown that the differences with the codes using other types of drift correlations derive from the relationship between steam quality and void fraction, which depends only on the velocity and density ratios between the two phases.

3.1.2 RADIAL FLOW–RATE DISTRIBUTION

The values in Fig. 8.1 show that the codes – with the obvious exception of ARROTTA – can predict reasonably well the flow–rate peaks in the macroelements adjacent to the peripheral shell. These high flow rates can be associated to the low values of the total pressure drops consequent to the presence of low–quality steam in these low–power channels (in the peripheral channels, this effect was counterbalanced by specifying a larger pressure drop in the inlet orifices). Once again, the QUANDRY–EN results deviate significantly; most likely, this is directly caused by a distorted power distribution shape (the peaking factor is 10 % lower than the mean) generated by the void fraction overestimate.

3.1.3 AXIAL POWER DISTRIBUTIONS

From the point of view of model intercomparison, the key feature of the normalized axial power shapes shown in Fig. 8.2, is the amplitude of the secondary peak, which is strongly dependent on the void fraction in the upper part of the core. It seems natural to look at the data of Fig. 8.2 in combination with the radial distributions of the outlet density shown in Fig. 8.3; however, the correlation is not so clear as one would expect, and a closer scrutiny will be needed to remove the ambiguities.

3.2 TRANSIENT RESULTS

Some of the most significant results from the transient calculations performed for Case D1 are discussed in the following paragraphs. To better visualize the dispersion in the results, Figures 8.4 through 8.6 show the time evolution of the variables, relative to the steady–state conditions.

3.2.1 TOTAL POWER

The time responses of the codes in terms of total power differ significantly from each other both in amplitudes and shapes notably in the first four seconds of the transient

(Fig. 8.4). The deviations are particularly large for KICOM and STAND, the two codes that use a quasi–static method to solve the time dependent diffusion equations (the other codes use nodal method variations). The methodological component may predominate in causing the discrepancies; all the more so, as the KICOM and STAND steady–state results are not so distant from the bunch.

3.2.2 OUTLET DENSITIES

In the first phase of the transient (0–2 seconds) a slight decrease was anticipated in the core–averaged outlet densities, with respect to the steady–state values. This behaviour, ascribable to the power increase that takes place until the inlet subcooling perturbation has propagated to the outlet, is not shown by DYNAS and TNK–XC (Fig. 8.5); which strongly suggests stability problems in the solution of the conservation equations in water. During the following phase – in principle, a monotonic increase to a new asymptotic state – the ARROTTA and KICOM shapes exhibit some oscillations. In the former case, these are fully coherent, in time and amplitude, with the oscillations in power shown in Fig. 8.4; in the latter, the simultaneous power oscillations are very small (not even visible in Fig. 8.4) and a concurrent numerical problem – presumably connected with the choice of the time step widths – must be invoked.

3.3.3 FUEL TEMPERATURES

The increases in core–averaged fuel temperatures at the end of the transient (Fig. 8.6) ranges from about 50 °C for KICOM and QUABOX–CUBBOX to about 120 °C for TNK–XC (the STAND data, representing the obviously lower pin surface temperatures, should be disregarded). Such a large dispersion is hard to justify in the context of the results for the other variables; it is surprising, for instance, that KICOM and QUABOX–CUBBOX produce virtually identical fuel temperature histories basing on significantly different power histories. Another puzzle, from the qualitative point of view, is represented by the shape of ARROTTA's response.

3.3.4 AXIAL POWER DISTRIBUTIONS

The axial distributions calculated at the time of maximum power (Fig. 8.7: results not available for all codes) show lower and flatter secondary peaks with respect to Fig. 8.2

These shapes are coherent with the relevant conditions (lower coolant density in the upper part of the core) and the overall agreement of the results is better than that observed at the initial steady–state.

4 CONCLUSIONS AND FUTURE WORK

The results obtained in the first phase of the PWR and BWR test can be considered very satisfactory. The intercomparison has been beneficial in different ways, given the different development or validation stages reached by the individual codes. Some participants have been able to spot weaknesses in their solutions (and in our specifications) and to take corrective measures. In fact, most solutions presented in this paper are "first iterations" – contributed after the NEA Specialists' Meeting on the benchmark – showing substantial improvements in terms of homogeneity of the results.

The suggested course of action for the second phase of the test is to perform sensitivity studies aimed at clarifying a few unresolved issues: an opportunity for these studies could be offered by the second BWR test problem E2, re–specified on a slower and more realistic core pressurization rate. As an extension of the PWR rod ejection benchmark, another reactivity accident starting at zero power – the uncontrolled withdrawal of control rods – is also in discussion.

That would complete the intercomparison exercise in the LWRCT context and break the ground for the challenging BWR stability benchmark (Ringhals 1 experimental data) licensed by the NEA Nuclear Science Committee to start in mid–1993.

Finally it is noted that a detailed summary and evaluation of all submitted data is available at the NEA DATA BANK.

5 REFERENCES

1 H. Finnemann and A. Galati,
"NEACRP 3-D LWR Core Transient Benchmark",
Final Specifications, NEACRP-L-335 (Revision 1), October 1991 (January 1992).

2 P.K. Hutt, Nuclear Electric, Berkeley, U.K.,
Letter to H. Finnemann, Subject: Revised PANTHER Results
for the NEACRP Rod Ejection Benchmark, Sept. 3, 1993.

3 H. Finnemann, H. Bauer, A. Galati, R. Martinelli
Results of LWR Core Transient Benchmarks
International Conference on Mathematical Methods and Supercomputing in
Nuclear Application, April 1993, Karlsruhe

Table 1 PWR Benchmark Cases A1–C2

CASE	Geometry	Initial State	Ejected CA
A1	Octant	HZP	Central
A2	Octant	HFP	Central
B1	Octant	HZP	Peripheral
B2	Octant	HFP	Peripheral
C1	Full Core	HZP	Peripheral
C2	Full Core	HFP	Peripheral

Remark: HFP = 2775 MW
HZP = 2775 W

Table 2.1 PWR. Participants of the Benchmark Problems A1–C2

Part.No.	Organization	Country	Code		A1	A2	B1	B2	C1	C2
1	TRACTEBEL	Belgium	OKAPI	(s)	X	X	X	X	X	X
				(a)	X		X		X	
2	VTT	Finland	BOREAS,TRAB		X	X	X	X	X	X
4	FRAMATOME	France	CESAR		X	X	X	X	X	X
5	EDF	France	COCCINELLE					X	X	
6	SIEMENS	Germany	PANBOX		X	X	X	X	X	X
7	GRS	Germany	QUABOX–CUBBOX		X	X	X	X	X	X
10	ENEL	Italy	QUANDRY–EN				X		X	
13	JAERI	Japan	REFLA/TRAC		X					
14	JAERI	Japan	THYDE–NEU					X		
19	ECN	Netherl.	PRORIA		X	X			X	X
20	NV KEMA	Netherl.	LWRSIM		X	X	X	X	X	X
21	ETS	Spain	SIMTRAN		X	X	X	X	X	X
23	INER	Taiwan	ARROTTA						X	X
24	NE Ber Lab	UK	PANTHER		X	X	X	X	X	X
total number		14			10	9	9	9	12	11

Table 2.2 PWR, Features of the Codes and Application in Benchmark

Organization	Code	Special Feature	Nodes/Ass. rad.	ax.
TRACTEBEL	OKAPI	1-D	1	16
VTT	BOREAS	Stationary	1	17 equid.
	TRAB	1-D	-	35
FRAMATOME	CESAR	finite diff.	4x4	16
EDF	COCCINELLE	finite diff.	4x4	16
SIEMENS	PANBOX		1	16
GRS	QUABOX-CUBBOX		1	16
ENEL	QUANDRY-EN		1	16
JAERI	REFLA/TRAC	R-Z	-	12
JAERI	THYDE-NEU	finite diff.	1	16
ECN	PRORIA	R-Z	-	12
NV KEMA	LWRSIM	Stationary	3x3	42 equid.
ETS	SIMTRAN		2x2	16
INER	ARROTTA		1	16
NE Ber Lab	PANTHER		1	16

Table 3.2 PWR, Transient Reference Solution

CASE	Nodes/Ass. rad.	ax.	No.time steps	Power	Time (s)	F_{xy}	F_Q	T_{Dop} (C)	T_{center} (C)
At Time of Power Maximum:									
A1	4	16	465	1.179	0.560	–	–	294.5	343.6
A2	4	16	34	1.080	0.10	–	–	546.5	1672.6
B1	4	16	465	2.441	0.517	–	–	301.4	328.9
B2	4	16	34	1.063	0.12	–	–	544.1	1577.0
C1	4	16	295	4.773	0.268	–	–	297.9	394.8
C2	4	16	34	1.071	0.10	–	–	546.4	1673.4
At Final Time t = 5 s:									
A1	4	16	465	0.196	5.0	–	–	324.3	673.3
A2	4	16	34	1.035	5.0	–	–	554.6	1691.8
B1	4	16	465	0.320	5.0	–	–	349.9	559.8
B2	4	16	34	1.038	5.0	–	–	552.0	1588.1
C1	4	16	295	0.146	5.0	–	–	315.9	676.1
C2	4	16	34	1.030	5.0	–	–	553.5	1733.5

Table 4.1 PWR. Effects of spatial mesh size and time step width (FP CASE A2)

	CASE	Nodes/Ass. rad.	ax.	No. time steps	Minimum time step	Max. Power	Time (s)	$T_{Dop.}$ (C)	T_{center} (C)
At Time of Power Maximum:									
PANTHER	A2	1	16	34	0.02	1.077	0.10	546.1	1670.7
		4	16	34	0.02	1.080	0.10 **)	546.5	1672.6
PANBOX	A2	1	16	95	0.01	1.080	0.10	552.1	1674.2
		1	16	190	0.005	1.080	0.10	552.2	1674.2
		1	16	96 *)	0.0008	1.080	0.12	552.1	1674.4
At Final Time t = 5 s:									
PANTHER	A2	1	16	34	0.02	1.034	5.0	554.2	1689.5
		4	16	34	0.02	1.035	5.0	554.6	1691.8
PANBOX	A2	1	16	95	0.01	1.036	5.0	560.7	1693.7
		1	16	190	0.005	1.036	5.0	560.7	1693.7
		1	16	96 *)	0.0008	1.035	5.0	560.7	1693.6

*) = automatic time step control

**) = a) the accuracy of the time of power maximum is obviously restricted to the minimum time step of 0.02 seconds
b) a previous PANTHER calculation with a minimum time step of 0.005 seconds (132 time steps) resulted in a time of power maximum of 0.12 seconds [3]

Table 4.2 PWR. Effects of spatial mesh size and time step width (HZP CASE A1)

	CASE	Nodes/Ass. rad.	ax.	No. time steps	Minimum time step	Max. Power	Time (s)	$T_{Dop.}$ (C)	T_{center} (C)
At Time of Power Maximum:									
PANTHER	A1	1	16	465	0.0025	0.899	0.647	293.6	339.7
		4	16	465	0.0025	1.179	0.560	294.5	343.6
PANBOX	A1	1	16	240	0.005	1.059	0.595	294.7	338.1
		1	16	480	0.0025	1.023	0.595	294.5	338.9
		1	16	325 *)	0.0032	1.033	0.600	294.5	339.3
At Final Time t = 5 s:									
PANTHER	A1	1	16	465	0.0025	0.195	5.0	323.9	665.0
		4	16	465	0.0025	0.196	5.0	324.3	673.3
PANBOX	A1	1	16	240	0.005	0.197	5.0	325.8	680.0
		1	16	480	0.0025	0.197	5.0	325.7	678.5
		1	16	325 *)	0.0032	0.197	5.0	325.8	679.8

*) = automatic time step control

Table 4.3 PWR . Effects of spatial mesh size and time step width (HZP CASE C1)

	CASE	Nodes/Ass. rad.	ax.	No. time steps	Minimum time step	Max. Power	Time (s)	$T_{Dop.}$ (C)	T_{center} (C)
At Time of Power Maximum:									
PANTHER	C1	1	16	295	0.002	5.572	0.264	298.8	412.7
		4	16	295	0.002	4.773	0.268	297.9	394.8
PANBOX	C1	1	16	240	0.005	5.432	0.270	298.4	388.4
		1	16	480	0.0025	4.936	0.265	298.5	388.5
		1	16	419 *)	0.0008	4.718	0.266	297.5	(381.5)
At Final Time t = 5 s:									
PANTHER	C1	1	16	295	0.002	0.150	5.0	317.0	696.8
		4	16	295	0.002	0.146	5.0	315.9	676.1
PANBOX	C1	1	16	240	0.005	0.15	5.0	317.6	694.0
		1	16	480	0.0025	0.15	5.0	317.7	694.9
		1	16	419 *)	0.0008	0.15	5.0	317.6	693.6

*) = automatic time step control

Table 5.1 PWR, Deviations: Critical Boron Concentration (ppm)

CASE:	A1	A2	B1	B2	C1	C2
REF.SOL.	567.700	1160.600	1254.600	1189.400	1135.300	1160.600
deviation (ppm):						
OKAPI (s)	-6.900	11.300	-4.700	6.800	-5.500	11.300
OKAPI (a)	-6.900	11.300	-4.700	6.800	-5.500	11.300
BOREAS/TRAB	134.600	-2.900	6.100	-8.100	22.300	-2.900
CESAR	20.300	-26.600	12.400	-26.400	14.700	-26.600
COCCINELLE					-48.700	-30.600
PANBOX	-2.900	2.000	-.900	.000	-1.900	2.100
QUABOX/CUBBOX	2.600	3.800	14.100	4.000	12.400	3.600
QUANDRY-EN			6.400		5.700	
REFLA/TRAC						
THYDE-NEU				70.600		
PRORIA	-236.700	43.400			-5.300	48.400
LWRSIM	18.900	12.600	4.000	9.900	6.500	12.600
SIMTRAN	1.100	2.400	3.500	2.300	3.600	2.400
ARROTTA					3.700	58.400
PANTHER	4.200	8.100	7.000	6.000	6.700	8.100
deviation (%):						
OKAPI (s)	-1.215	.974	-.375	.572	-.484	.974
OKAPI (a)	-1.215	.974	-.375	.572	-.484	.974
BOREAS/TRAB	23.710	-.250	.486	-.681	1.964	-.250
CESAR	3.576	-2.292	.988	-2.220	1.295	-2.292
COCCINELLE					-4.290	-2.637
PANBOX	-.511	.172	-.072	.000	-.167	.181
QUABOX/CUBBOX	.458	.327	1.124	.336	1.092	.310
QUANDRY-EN			.510		.502	
REFLA/TRAC						
THYDE-NEU				5.936		
PRORIA	-41.695	3.739			-.467	4.170
LWRSIM	3.329	1.086	.319	.832	.573	1.086
SIMTRAN	.194	.207	.279	.193	.317	.207
ARROTTA					.326	5.032
PANTHER	.740	.698	.558	.504	.590	.698

Table 5.2 PWR, Deviations: Nodal Power Peaking Factor

CASE:	A1	A2	B1	B2	C1	C2
REF.SOL.	2.874	2.221	1.932	2.109	2.187	2.221
deviation:						
OKAPI (s)	.007	.033	-.005	.015	-.003	.033
OKAPI (a)	.007	.033	-.005	.015	-.003	.033
BOREAS/TRAB	.506	.019	.088	-.009	.053	.019
CESAR	.246	-.041	.158	-.049	.293	-.041
PANBOX	-.028	-.014	-.005	-.016	-.003	-.015
QUABOX/CUBBOX	-.032	-.012	.003	-.003	.011	-.011
QUANDRY-EN			-.002		-.003	
LWRSIM	.120	.042	.063	.017	.087	.042
ARROTTA					-.042	.161
PANTHER	-.028	-.005	-.006	-.006	-.004	-.005
deviation (%):						
OKAPI (s)	.244	1.486	-.259	.711	-.137	1.485
OKAPI (a)	.244	1.486	-.259	.711	-.137	1.486
BOREAS/TRAB	17.606	.855	4.555	-.427	2.423	.855
CESAR	8.559	-1.846	8.178	-2.323	13.397	-1.846
PANBOX	-.974	-.630	-.259	-.759	-.137	-.675
QUABOX/CUBBOX	-1.113	-.540	.155	-.142	.503	-.495
QUANDRY-EN			-.104		-.137	
LWRSIM	4.175	1.891	3.261	.806	3.978	1.891
ARROTTA					-1.920	7.249
PANTHER	-.974	-.225	-.311	-.284	-.183	-.225

Table 5.3 PWR, Homogeneous Power Peaking Factor

CASE:	A1	A2	B1	B2	C1	C2
! no reference solution available !						
results:						
OKAPI (s)	3.185	2.525	2.289	2.347	2.436	2.525
OKAPI (a)	3.185	2.525	2.289	2.347	2.436	2.525
COCCINELLE					2.537	2.391
PANBOX	3.201	2.556	2.229	2.348	2.519	2.518
REFLA/TRAC	3.203					
THYDE-NEU				2.181		
PRORIA	1.460	2.360			1.450	2.590
LWRSIM	3.202	2.319	2.045	2.164	2.400	2.319
SIMTRAN	3.147	2.431	2.193	2.324	2.508	2.431
PANTHER						

Table 5.4 PWR, Deviations: Reactivity Release (pcm)

CASE:	A1	A2	B1	B2	C1	C2
REF.SOL.	822.000	90.000	831.000	99.000	958.000	78.000
deviation (pcm):						
CESAR	-33.000	-4.000	-20.000	8.000	-19.000	2.000
PANBOX	-12.000	-1.000	-8.000	2.000	-7.000	2.000
SIMTRAN	-12.000	.000	.000	2.000	3.000	3.000
PANTHER	-15.000	-3.000	1.000	1.000	7.000	1.000
deviation (%):						
CESAR	-4.015	-4.444	-2.407	8.081	-1.933	2.564
PANBOX	-1.460	-1.111	-.963	2.020	-.731	2.564
SIMTRAN	-1.460	.000	.000	2.020	.313	3.846
PANTHER	-1.825	-3.333	.120	1.010	.731	1.282

Table 5.5 PWR. Deviations: Time of Power Maximum (s)

CASE:	A1	A2	B1	B2	C1	C2
REF.SOL.	.560	.100	.520	.120	.270	.100
deviation (s):						
OKAPI (s)	.030	-.020	-.020	-.020	-.030	.000
OKAPI (a)	.020		-.040		-.030	
BOREAS/TRAB	.070	.110	-.030	.290	.010	.110
CESAR	.210	.000	.090	-.020	.030	.000
COCCINELLE					.050	-.020
PANBOX	.040	.000	.000	-.010	.000	.000
QUABOX/CUBBOX	.030	-.010	-.100	-.040	.030	-.010
QUANDRY-EN			-.020		-.010	
REFLA/TRAC	-.410					
THYDE-NEU				.690		
PRORIA	1.240	.000				.000
SIMTRAN	.080	.000	.000	-.010	.000	.000
ARROTTA					-.010	-.020
PANTHER	.090	.000	.000	.000	-.010	.020
deviation (%):						
OKAPI (s)	5.357	-20.000	-3.846	-16.667	-11.111	.000
OKAPI (a)	3.571		-7.692		-11.111	
BOREAS/TRAB	12.500	110.000	-5.769	241.667	3.704	110.000
CESAR	37.500	.000	17.308	-16.667	11.111	.000
COCCINELLE					18.519	-20.000
PANBOX	7.143	.000	.000	-8.333	.000	.000
QUABOX/CUBBOX	5.357	-10.000	-19.231	-33.333	11.111	-10.000
QUANDRY-EN			-3.846		-3.704	
REFLA/TRAC	-73.214					
THYDE-NEU				575.000		
PRORIA	221.429	.000				.000
SIMTRAN	14.286	.000	.000	-8.333	.000	.000
ARROTTA					-3.704	-20.000
PANTHER	16.071	.000	.000	.000	-3.704	20.000

Table 5.6 PWR, Deviations: Power Maximum (% of P/2775 MW)

CASE:	A1	A2	B1	B2	C1	C2
REF.SOL.	117.900	108.000	244.100	106.300	477.300	107.100
deviation (% of P/2775 MW):						
OKAPI (s)	-41.500	-.400	5.900	-3.300	-172.500	-.700
OKAPI (a)	-.400		49.800		144.000	
BOREAS/TRAB	29.600	-.200	7.700	-.200	783.800	-.100
CESAR	-54.400	1.100	-74.700	.700	-151.000	1.500
COCCINELLE					-197.600	-.100
PANBOX	-14.600	.000	-4.100	.300	-5.500	.300
QUABOX/CUBBOX	14.500	.900	306.600	1.100	621.700	1.900
QUANDRY-EN			2.200		48.900	
THYDE-NEU				-.200		
PRORIA	-86.100	.300				.200
SIMTRAN	-33.400	.300	-13.000	.300	-36.600	.600
ARROTTA					16.200	1.000
PANTHER	-28.000	-.300	20.000	.100	79.900	.100
deviation (%):						
OKAPI (s)	-35.199	-.370	2.417	-3.104	-36.141	-.654
OKAPI (a)	-.339		20.401		30.170	
BOREAS/TRAB	25.106	-.185	3.154	-.188	164.215	-.093
CESAR	-46.141	1.019	-30.602	.659	-31.636	1.401
COCCINELLE					-41.400	-.093
PANBOX	-12.383	.000	-1.680	.282	-1.152	.280
QUABOX/CUBBOX	12.299	.833	125.604	1.035	130.254	1.774
QUANDRY-EN			.901		10.245	
THYDE-NEU				-.188		
PRORIA	-73.028	.278				.187
SIMTRAN	-28.329	.278	-5.326	.282	-7.668	.560
ARROTTA					3.394	.934
PANTHER	-23.749	-.278	8.193	.094	16.740	.093

Table 5.7 PWR. Deviations: Final Power (% of P/2775 MW) at t = 5 s

CASE:	A1	A2	B1	B2	C1	C2
REF.SOL.	19.600	103.500	32.000	103.800	14.600	103.000
deviation (% of P/2775 MW):						
OKAPI (s)	-.200	-.700	-1.500	-2.000	1.100	-.500
OKAPI (a)	4.900		.400		6.900	
BOREAS/TRAB	13.800	.800	4.000	.700	27.900	.900
CESAR	-2.600	-.100	-3.900	.000	-1.900	.000
COCCINELLE					.200	.100
PANBOX	.100	.100	.500	.300	.400	.200
QUABOX/CUBBOX	-.100	.700	1.200	.800	.600	1.100
QUANDRY-EN			-7.500		-2.500	
THYDE-NEU				1.000		
PRORIA	5.100	.200				.600
SIMTRAN	1.200	.100	1.500	.200	.900	.200
ARROTTA					2.800	.000
PANTHER	-.100	-.100	.500	.100	.400	.100
deviation (%):						
OKAPI (s)	-1.020	-.676	-4.688	-1.927	7.534	-.485
OKAPI (a)	25.000		1.250		47.260	
BOREAS/TRAB	70.408	.773	12.500	.674	191.096	.874
CESAR	-13.265	-.097	-12.187	.000	-13.014	.000
COCCINELLE					1.370	.097
PANBOX	.510	.097	1.563	.289	2.740	.194
QUABOX/CUBBOX	-.510	.676	3.750	.771	4.110	1.068
QUANDRY-EN			-23.438		-17.123	
THYDE-NEU				.963		
PRORIA	26.020	.193				.583
SIMTRAN	6.122	.097	4.688	.193	6.164	.194
ARROTTA					19.178	.000
PANTHER	-.510	-.097	1.563	.096	2.740	.097

Table 5.8 PWR. Deviations: Final Steady–State Power (% of P/2775 MW)

CASE:	A1	A2	B1	B2	C1	C2
REF.SOL.	26.300	103.600	41.600	104.100	20.600	103.200
deviation (% of P/2775 MW):						
PANBOX	-.100	.100	.500	.300	.600	.100
SIMTRAN	1.300	.100	1.400	.100	1.200	.100
PANTHER	-.100	.000	.400	.100	.600	.000
deviation (%):						
PANBOX	-.380	.097	1.202	.288	2.913	.097
SIMTRAN	4.943	.097	3.365	.096	5.825	.097
PANTHER	-.380	.000	.962	.096	2.913	.000

Table 5.9 PWR, Deviation: Final Core Averaged Doppler Temperature (°C)

CASE:	A1	A2	B1	B2	C1	C2
REF. SOL.	324.300	554.600	349.900	552.000	315.900	553.500
deviation (°C):						
OKAPI (s)	-.900	-1.400	-1.200	-3.900	1.200	-1.100
OKAPI (a)	10.500		2.800		14.700	
BOREAS/TRAB	33.100	20.200	14.700	25.600	69.300	20.300
CESAR	-2.100	40.700	-2.300	38.100	-1.400	40.800
COCCINELLE					.700	2.500
PANBOX	1.500	6.100	3.200	6.400	1.700	6.100
QUABOX/CUBBOX			9.400	13.400		
QUANDRY-EN			2.500		2.600	
THYDE-NEU				53.000		
PRORIA	8.900	14.800				19.300
LWRSIM						
SIMTRAN	3.500	12.000	5.600	12.000	3.000	12.100
ARROTTA					-7.900	-127.500
PANTHER	-.400	-.400	1.300	-.100	1.100	-.100
deviation (%):						
OKAPI (s)	-.278	-.252	-.343	-.707	.380	-.199
OKAPI (a)	3.238		.800		4.653	
BOREAS/TRAB	10.207	3.642	4.201	4.638	21.937	3.668
CESAR	-.648	7.339	-.657	6.902	-.443	7.371
COCCINELLE					.222	.452
PANBOX	.463	1.100	.915	1.159	.538	1.102
QUABOX/CUBBOX			2.686	2.428		
QUANDRY-EN			.714		.823	
THYDE-NEU				9.601		
PRORIA	2.744	2.669				3.487
LWRSIM						
SIMTRAN	1.079	2.164	1.600	2.174	.950	2.186
ARROTTA					-2.501	-23.035
PANTHER	-.123	-.072	.372	-.018	.348	-.018

Table 5.10 PWR, Deviations: Final Maximum Fuel Centerline Temperature (°C)

CASE:	A1	A2	B1	B2	C1	C2
REF.SOL.	673.300	1691.800	559.800	1588.100	676.100	1733.500
deviation (°C):						
OKAPI (s)	-19.300	-5.200	-7.300	-7.000	-4.500	-48.500
OKAPI (a)	133.100		15.100		225.000	
CESAR	-45.300	4.300	-30.000	-4.000	-18.400	-5.700
COCCINELLE					12.400	57.900
PANBOX	6.500	1.800	8.600	-.400	17.500	5.500
REFLA/TRAC	-4.200					
THYDE-NEU				-9.800		
SIMTRAN	25.600	19.800	16.900	10.900	34.600	26.800
PANTHER	-8.300	-2.300	4.900	-2.600	20.700	-.200
deviation (%):						
OKAPI (s)	-2.866	-.307	-1.304	-.441	-.666	-2.798
OKAPI (a)	19.768		2.697		33.279	
CESAR	-6.728	.254	-5.359	-.252	-2.721	-.329
COCCINELLE					1.834	3.340
PANBOX	.965	.106	1.536	-.025	2.588	.317
REFLA/TRAC	-.624					
THYDE-NEU				-.617		
SIMTRAN	3.802	1.170	3.019	.686	5.118	1.546
PANTHER	-1.233	-.136	.875	-.164	3.062	-.012

Table 5.11 PWR, Deviations: Final Coolant Outlet Temperature (°C)

CASE:	A1	A2	B1	B2	C1	C2
REF.SOL.	293.100	324.600	297.600	324.700	291.500	324.500
deviation (°C):						
OKAPI (s)	-.300	-.100	-.400	-.500	.200	.000
OKAPI (a)	1.700		.300		2.600	
BOREAS/TRAB	4.800	.500	1.400	.400	10.600	.500
CESAR	-.900	-.100	-1.300	-.100	-.600	-.100
COCCINELLE						
PANBOX	.100	.500	.300	.500	.200	.500
QUABOX/CUBBOX	-.100	.300	.300	.500	-.100	.200
QUANDRY-EN			-4.900		-2.200	
THYDE-NEU				1.300		
REFLA/TRAC	8.500					
PRORIA	.200	-3.500				-3.500
LWRSIM						
SIMTRAN	.200	-.100	.300	-.100	.200	-.100
ARROTTA					1.000	.000
PANTHER	-.100	.100	.200	.100	.200	.100
deviation (%):						
OKAPI (s)	-.102	-.031	-.134	-.154	.069	.000
OKAPI (a)	.580		.101		.892	
BOREAS/TRAB	1.638	.154	.470	.123	3.636	.154
CESAR	-.307	-.031	-.437	-.031	-.206	-.031
COCCINELLE						
PANBOX	.034	.154	.101	.154	.069	.154
QUABOX/CUBBOX	-.034	.092	.101	.154	-.034	.062
QUANDRY-EN			-1.647		-.755	
THYDE-NEU				.400		
REFLA/TRAC	2.900					
PRORIA	.068	-1.078				-1.079
LWRSIM						
SIMTRAN	.068	-.031	.101	-.031	.069	-.031
ARROTTA					.343	.000
PANTHER	-.034	.031	.067	.031	.069	.031

Table 5.12 PWR. CASE C1: Deviations: Radial Power Distribution at Time of Power Maximum in Axial Layer 13 (Along the Horizontal Traverse)

REF. SOL.:	.024	.021	.049	.054	.041	.022	.037	.038	.100	.138	.429	.757	.991	1.000	.846
deviation:															
OKAPI (s)	.000	.000	-.001	-.002	-.001	.000	-.001	.000	-.001	-.001	-.003	-.004	-.003	.000	.000
OKAPI (a)	-.002	-.001	-.004	-.004	-.003	-.001	-.002	-.001	-.002	-.003	-.006	-.007	-.005	.000	.000
OCESAR	.003	.000	.001	.002	.000	.000	.000	-.001	-.002	-.007	-.018	-.009	-.035	.000	.010
COCCINELLE	-.001	.003	.008	.008	.008	.005	.005	.005	.009	.011	.025	.000	.009	-.071	-.111
PANBOX	.001	.000	-.001	.000	.000	.000	-.001	.000	-.001	-.002	-.005	-.008	-.007	.000	.004
QUABOX/CUBBOX	-.004	-.007	-.015	-.013	-.012	-.006	-.008	-.009	-.014	-.028	-.053	-.030	-.074	.000	.037
QUANDRY-EN	.001	.000	-.001	-.001	-.001	.000	-.001	-.001	-.002	-.003	-.009	-.009	-.011	.000	.007
SIMTRAN	.000	.000	-.001	-.001	-.001	.000	-.001	-.001	-.002	-.003	-.007	-.008	-.010	.000	.009
ARROTTA	.004	.004	.006	.006	.004	.003	.003	.002	.003	.003	-.003	-.006	-.009	.000	.002
PANTHER	.001	.001	.000	.000	.000	.000	-.001	-.001	-.002	-.003	-.009	-.009	-.012	.000	.008
deviation (%):															
OKAPI (s)	-.4	-1.0	-2.9	-2.8	-2.4	-.9	-2.4	-1.1	-.9	-.8	-.7	-.5	-.3	.0	.0
OKAPI (a)	-6.7	-6.7	-8.4	-8.1	-7.3	-5.0	-5.4	-3.2	-2.3	-1.9	-1.4	-.9	-.5	.0	.0
CESAR	12.5	.0	2.0	3.7	.0	.0	.0	-2.6	-2.0	-5.1	-4.2	-1.2	-3.5	.0	1.2
COCCINELLE	-4.2	14.3	16.3	14.8	19.5	22.7	13.5	13.2	9.0	8.0	5.8	.0	.9	-7.1	-13.1
PANBOX	4.2	.0	-2.0	.0	.0	.0	-2.7	.0	-1.0	-1.4	-1.2	-1.1	-.7	.0	.5
QUABOX/CUBBOX	-16.7	-33.3	-30.6	-24.1	-29.3	-27.3	-21.6	-23.7	-14.0	-20.3	-12.4	-4.0	-7.5	.0	4.4
QUANDRY-EN	4.2	.0	-2.0	-1.9	-2.4	.0	-2.7	-2.6	-2.0	-2.2	-2.1	-1.2	-1.1	.0	.8
SIMTRAN	.0	.0	-2.0	-1.9	-2.4	.0	-2.7	-2.6	-2.0	-2.2	-1.6	-1.1	-1.0	.0	1.1
ARROTTA	16.7	19.0	12.2	11.1	9.8	13.6	8.1	5.3	3.0	2.2	-.7	-.8	-.9	.0	.2
PANTHER	4.2	4.8	.0	.0	.0	.0	-2.7	-2.6	-2.0	-2.2	-2.1	-1.2	-1.2	.0	.9

Table 5.13 PWR, CASE C2: Deviations: Radial Power Distribution at Time of Power Maximum in Axial Layer 13 (Along the Horizontal Traverse)

REF. SOL.:	.266	.229	.526	.663	.662	.618	.518	.318	.565	.722	.844	.963	1.000	.950	.799
deviation:															
OKAPI (s)	-.082	-.054	-.090	-.113	-.094	-.013	-.020	-.010	.022	.076	.004	-.001	.000	-.083	-.124
CESAR	.017	-.008	-.022	-.004	-.033	-.073	-.049	-.029	-.053	-.076	-.027	.012	-.016	.050	.059
COCCINELLE	-.033	.001	.009	.005	.033	.004	.024	.020	.022	-.003	.032	-.010	.000	-.053	-.087
PANBOX	.003	-.001	-.004	-.007	-.009	-.010	-.007	-.006	-.009	-.010	-.008	-.006	.000	.010	.010
QUABOX/CUBBOX	.048	-.010	.007	.060	-.012	-.041	-.036	-.041	-.047	-.058	-.041	.037	-.044	.050	.077
SIMTRAN	-.001	.000	-.005	-.005	-.013	-.011	-.016	-.006	-.016	-.008	-.008	.005	.000	.005	.004
ARROTTA	.007	.002	-.014	-.007	-.017	-.062	-.033	-.010	-.032	-.062	-.005	.010	.000	.032	.034
PANTHER	.007	.001	-.001	-.003	-.007	-.005	-.006	-.005	-.007	-.005	-.007	.000	.000	.015	.014
deviation (%):															
OKAPI (s)	-30.9	-23.8	-17.0	-17.0	-14.1	-2.1	-3.8	-3.1	3.9	10.6	.4	-.1	.0	-8.8	-15.5
CESAR	6.4	-3.5	-4.2	-.6	-5.0	-11.8	-9.5	-9.1	-9.4	-10.5	-3.2	1.2	-1.6	5.3	7.4
COCCINELLE	-12.4	.4	1.7	.8	5.0	.6	4.6	6.3	3.9	-.4	3.8	-1.0	.0	-5.6	-10.9
PANBOX	1.1	-.4	-.8	-1.1	-1.4	-1.6	-1.4	-1.9	-1.6	-1.4	-.9	-.6	.0	1.1	1.3
QUABOX/CUBBOX	18.0	-4.4	1.3	9.0	-1.8	-6.6	-6.9	-12.9	-8.3	-8.0	-4.9	3.8	-4.4	5.3	9.6
SIMTRAN	-.4	.0	-1.0	-.8	-2.0	-1.8	-3.1	-1.9	-2.8	-1.1	-.9	.5	.0	.5	.5
ARROTTA	2.6	.9	-2.7	-1.1	-2.6	-10.0	-6.4	-3.1	-5.7	-8.6	-.6	1.0	.0	3.4	4.3
PANTHER	2.6	.4	-.2	-.5	-1.1	-.8	-1.2	-1.6	-1.2	-.7	-.8	.0	.0	1.6	1.8

Table 6 BWR, Participants of the BWR Benchmark Case D1 and Steady – State K_{eff}

Part.-No.	Organization	Country	Code	Steady-State K_{eff}
23	INER	Taiwan	ARROTTA	0.99999
18	NFI-SIEMENS	Japan	DYNAS	0.98563
31	SIEMENS	USA	TNK-XC	0.98764
17	Osaka Un.	Japan	KICOM	0.98440
2	VTT	Finland	BOREAS	0.98035
10	ENEL	Italy	QUANDRY-EN	0.96788
15	Hitachi	Japan	STAND	0.99100
7	GRS	Germany	QUABOX-CUBBOX	0.98639
total number		8	8	

Fig. 1.1 PWR Core Map

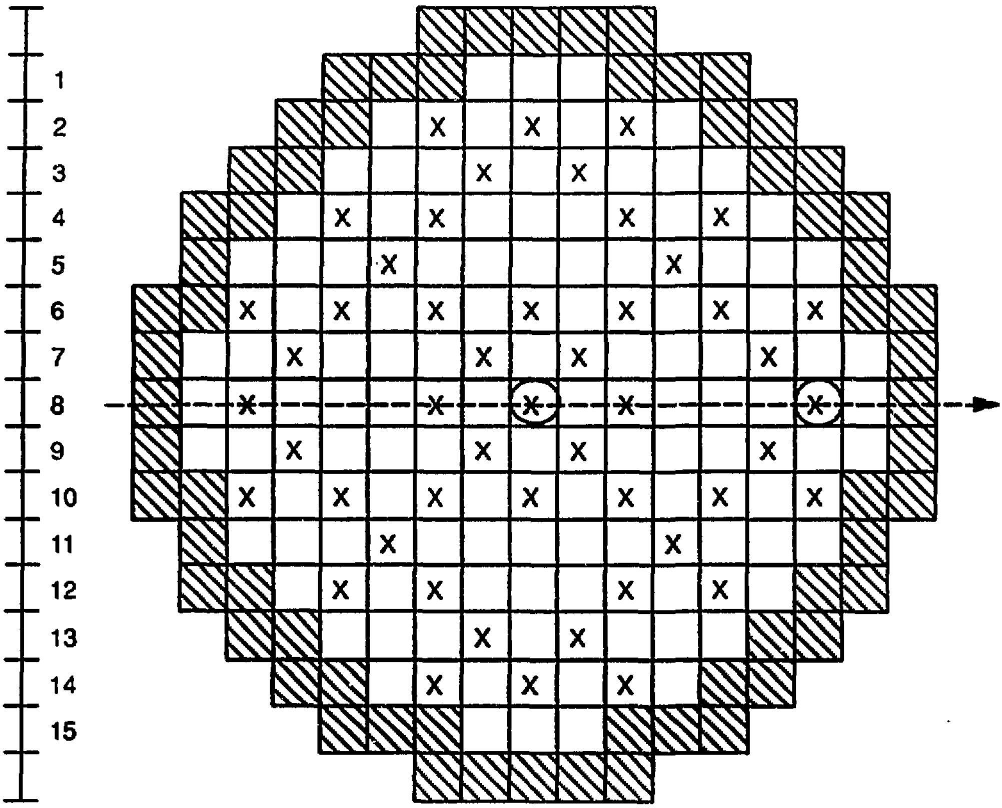

= Radial Reflector Element

= Fuel Assembly

X = Control Assembly

(X) = Central or Peripheral CA to be Ejected

= Horizontal Traverse

Fig. 1.2 BWR Core Map

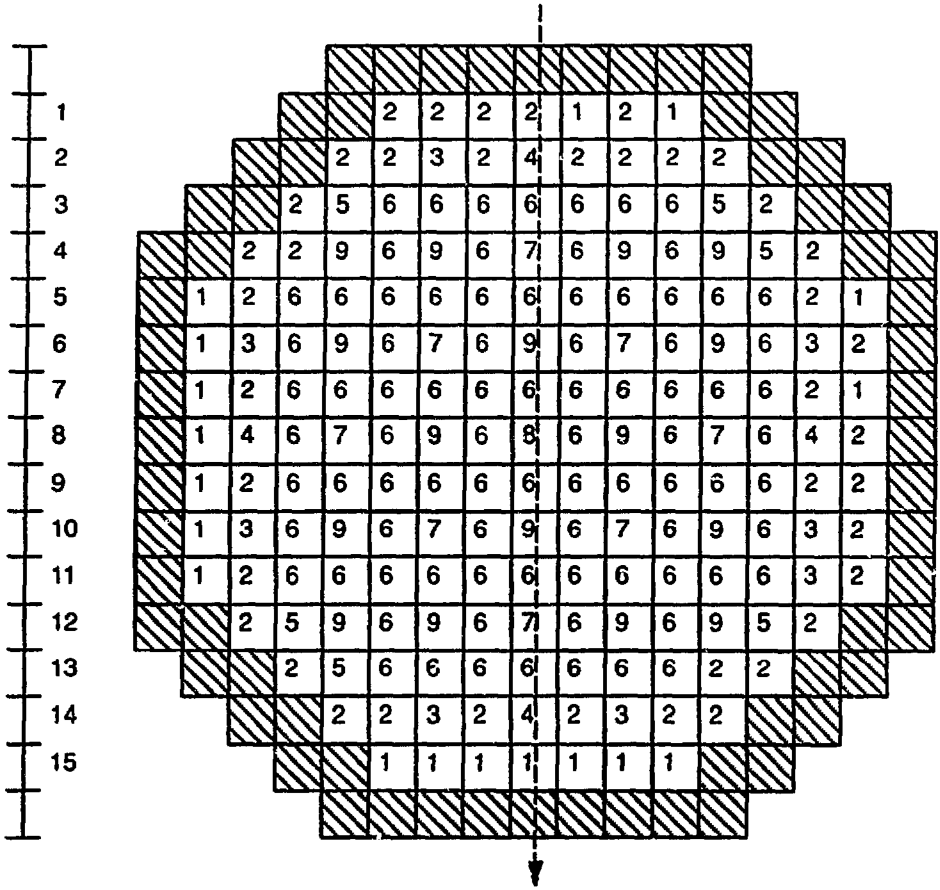

= Radial Reflector Element   = Fuel Assembly

= Vertical Traverse

PWR: Key to Figures 2.1–7.6

----	REFERENCE
1 s	OKAPI (s)
1 a	OKAPI (a)
2	TRAB
4	CESAR
5	COCCINELLE
6	PANBOX
7	QUABOX–CUBBOX
10	QUANDRY–EN
13	REFLA/TRAC
14	THYDE–NEU
19	PRORIA
20	LWRSIM
21	SIMTRAN
23	ARROTTA
24	PANTHER

Fig. 2.1 PWR, CASE A1, Total Reactor Power versus Time

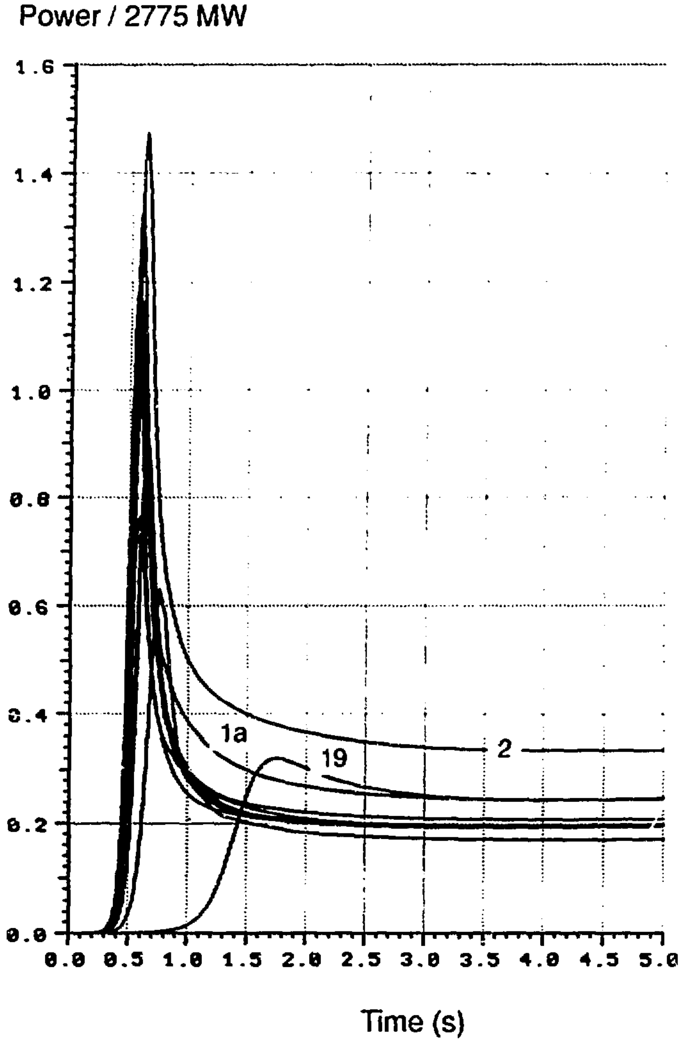

Fig. 2.2 PWR, CASE A1, Total Reactor Power versus Time

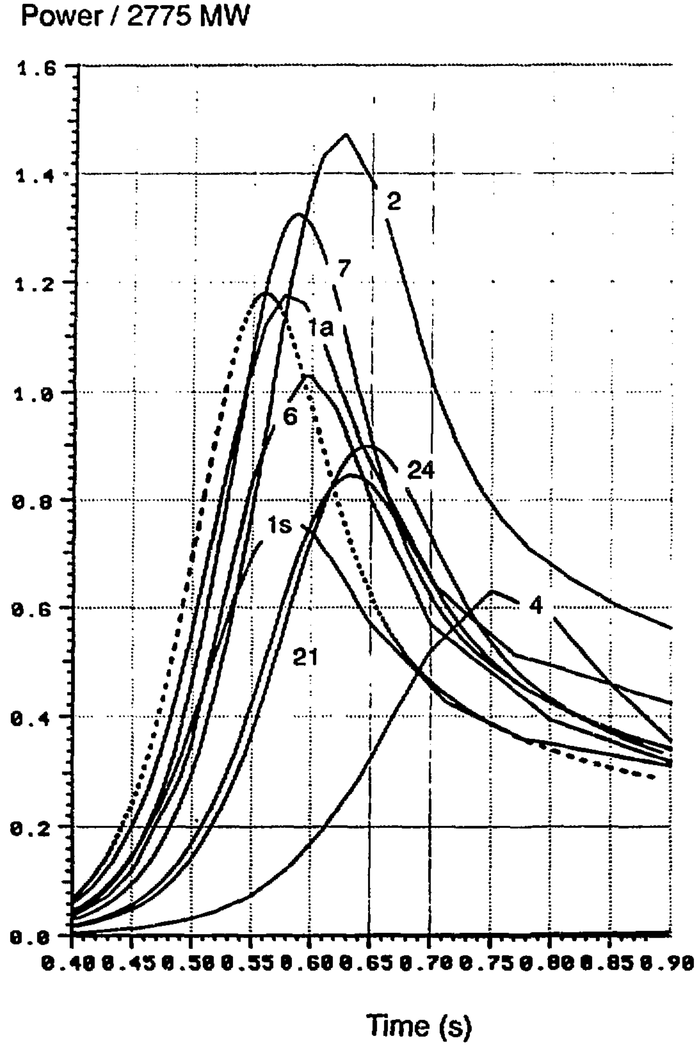

Fig. 2.3 PWR, CASE A1, Doppler Temperature versus Time

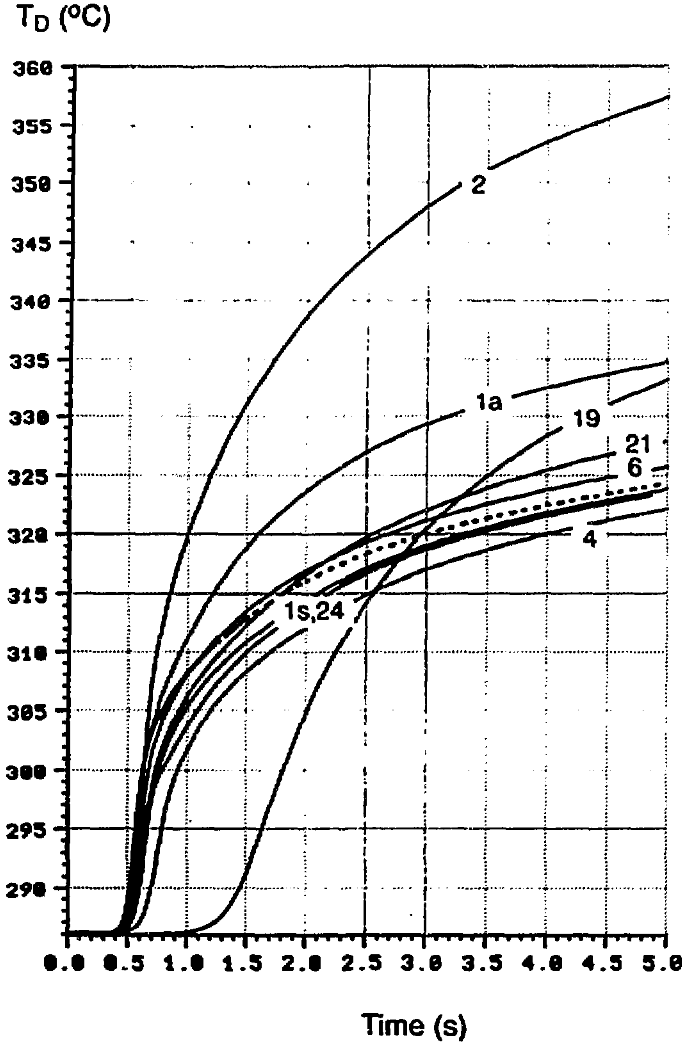

Fig. 2.4 PWR, CASE A1, Maximum Nodal Fuel Centerline Temperature versus Time

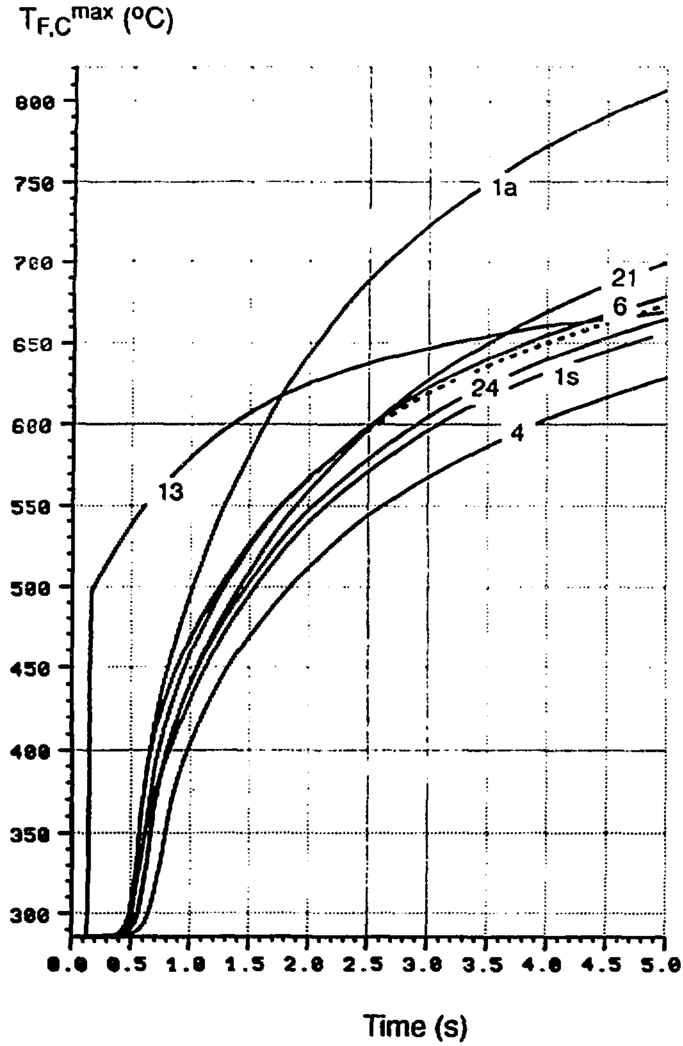

Fig. 2.5 PWR, CASE A1, Maximum Node Averaged Fuel Temperature versus Time

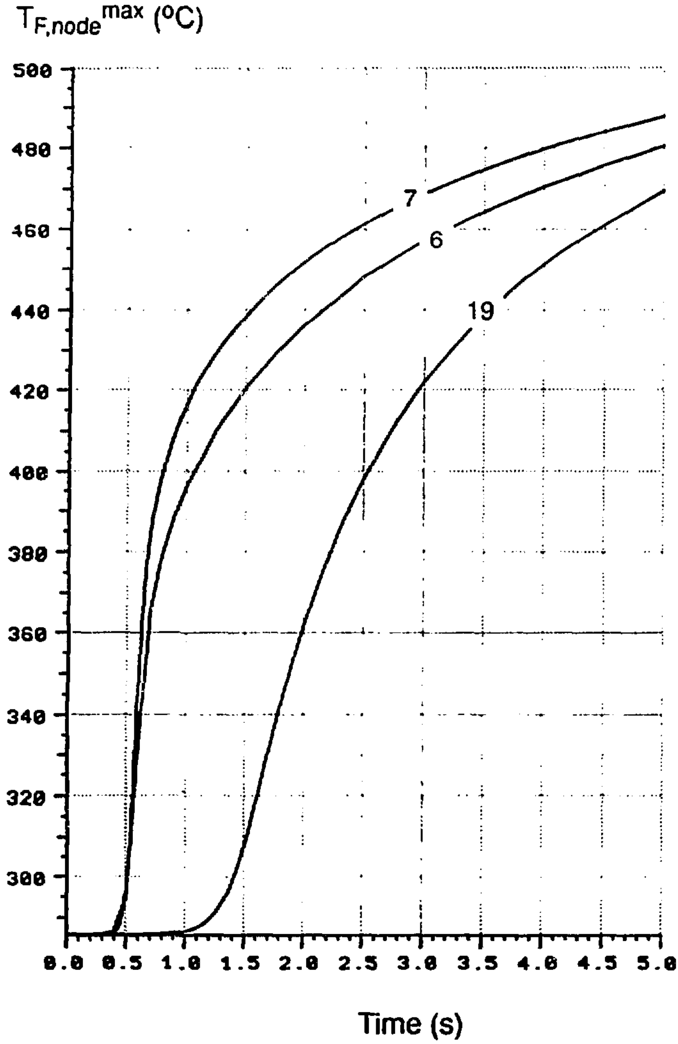

Fig. 2.6 PWR, CASE A1, Coolant Exit Temperature versus Time

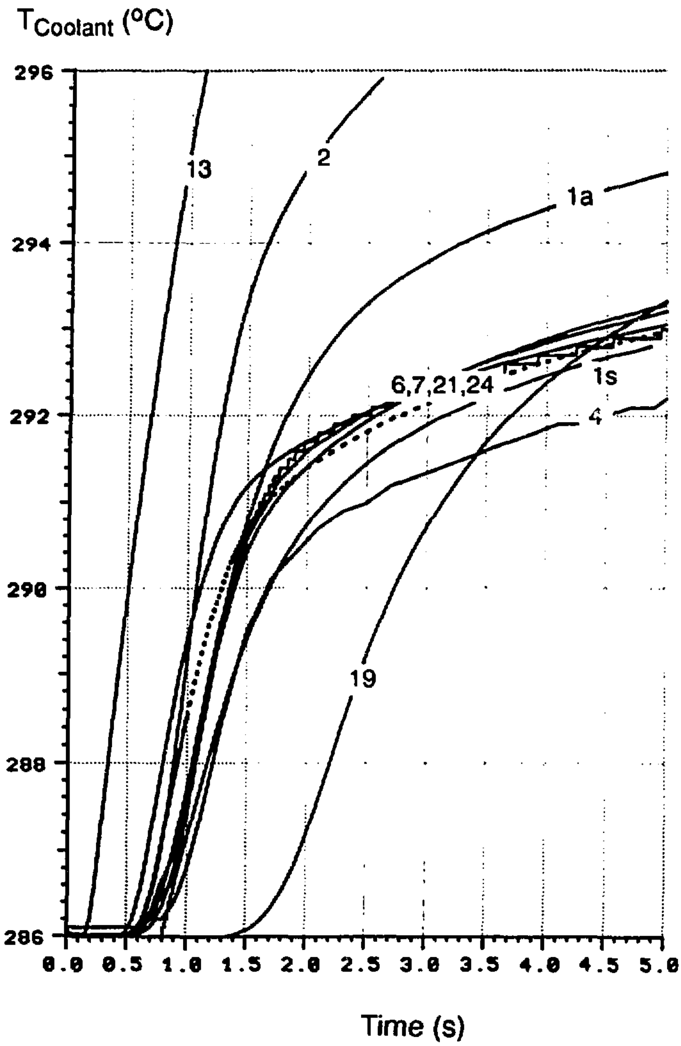

Fig. 3.1 PWR, CASE A2, Total Reactor Power versus Time

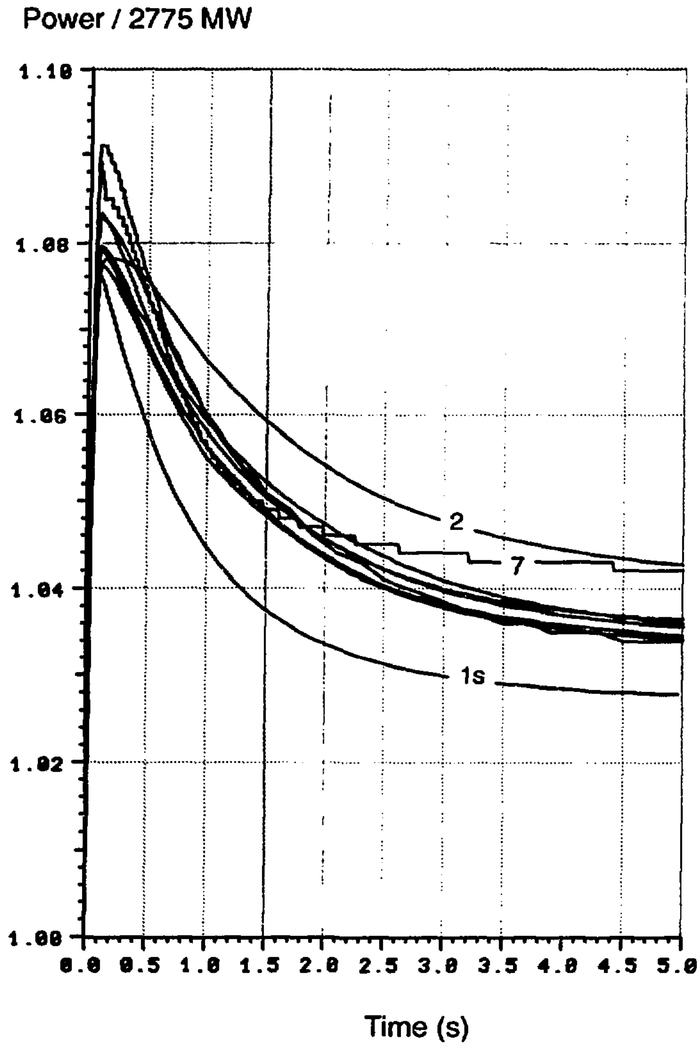

Fig. 3.2 PWR, CASE A2, Total Reactor Power versus Time

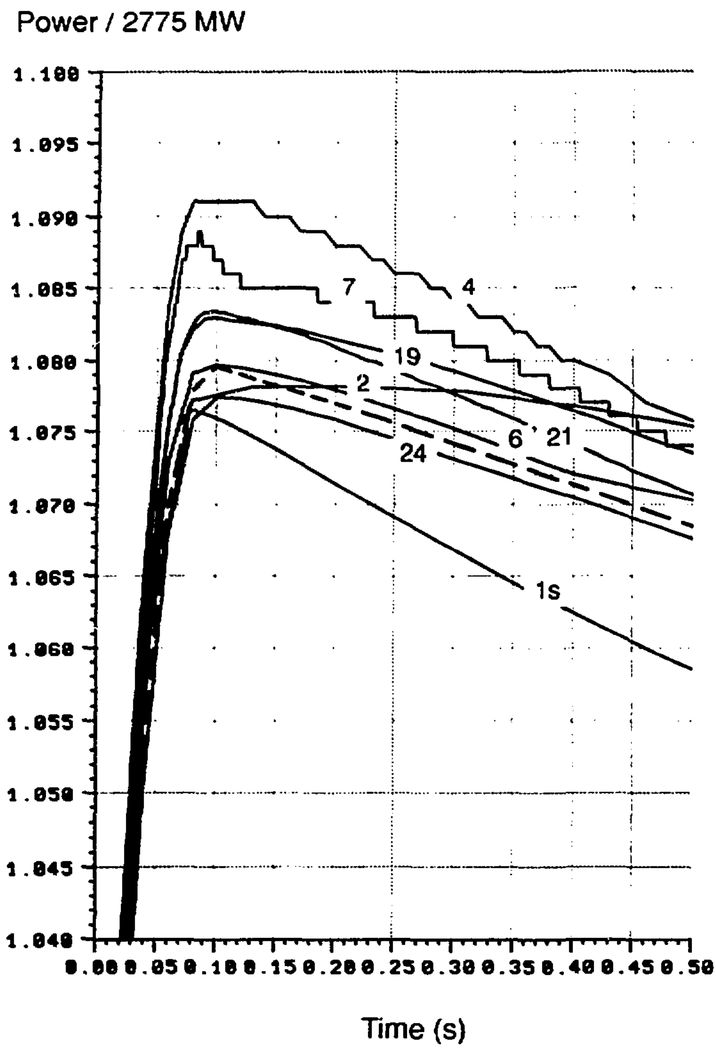

Fig. 3.3 PWR, CASE A2, Doppler Temperature versus Time

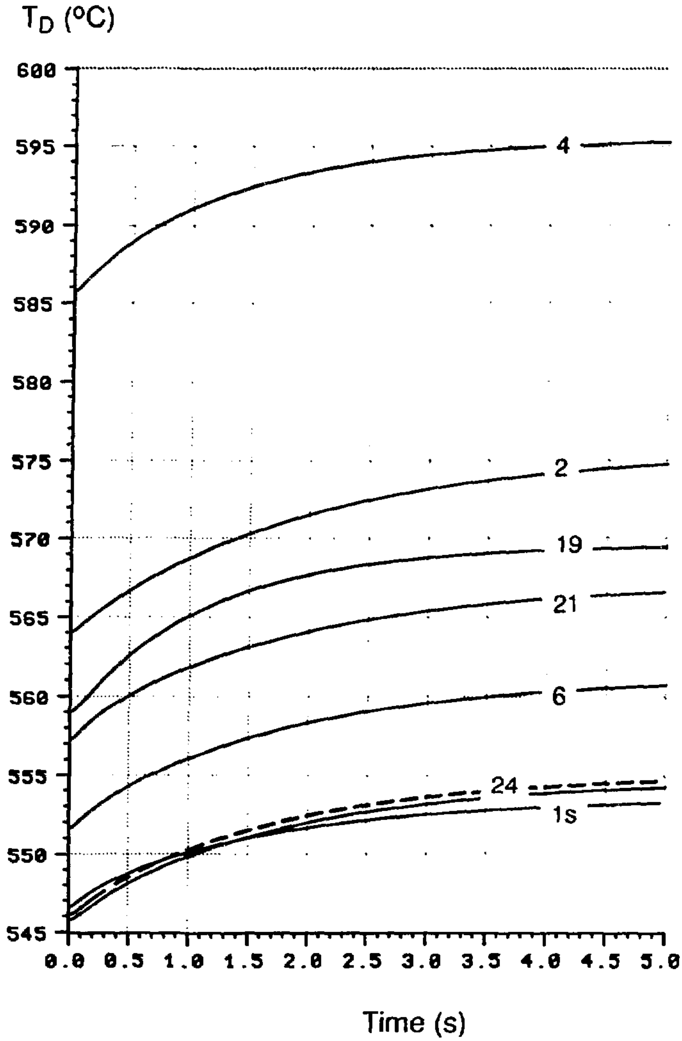

Fig. 3.4 PWR, CASE A2, Maximum Nodal Fuel Centerline Temperature versus Time

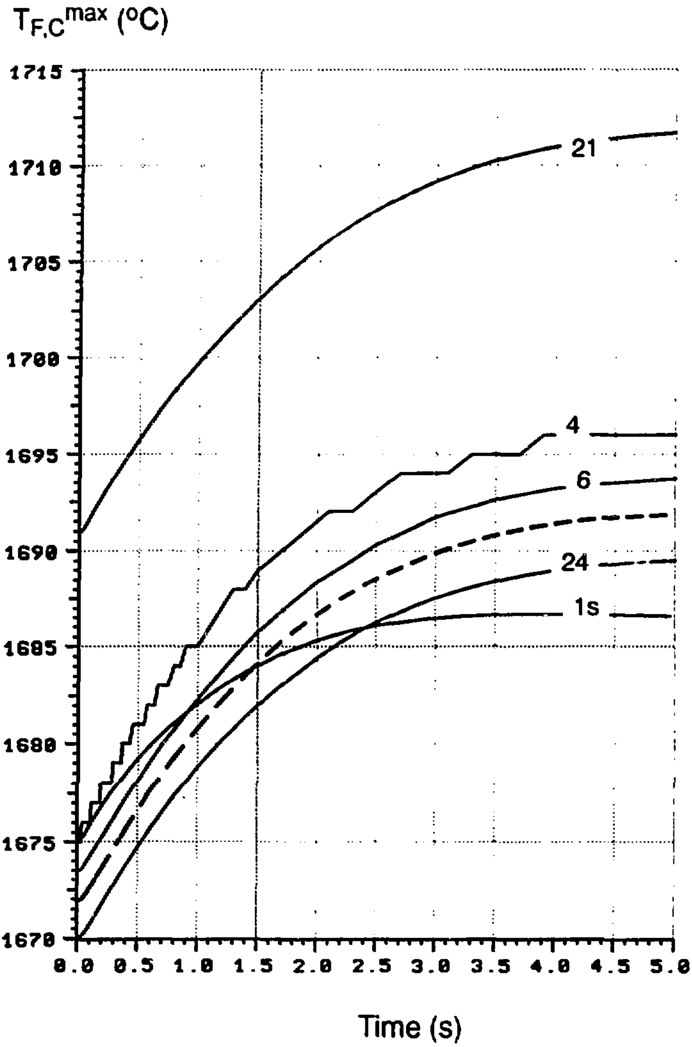

Fig. 3.5 PWR, CASE A2, Maximum Node Averaged Fuel Temperature versus Time

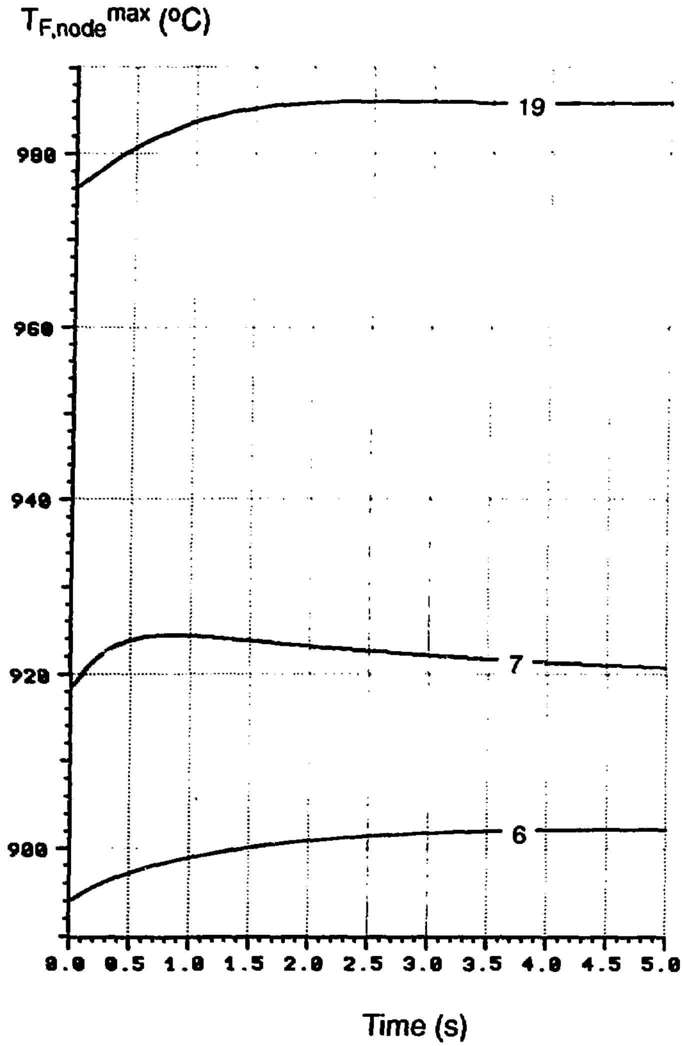

Fig. 3.6 PWR, CASE A2, Coolant Exit Temperature versus Time

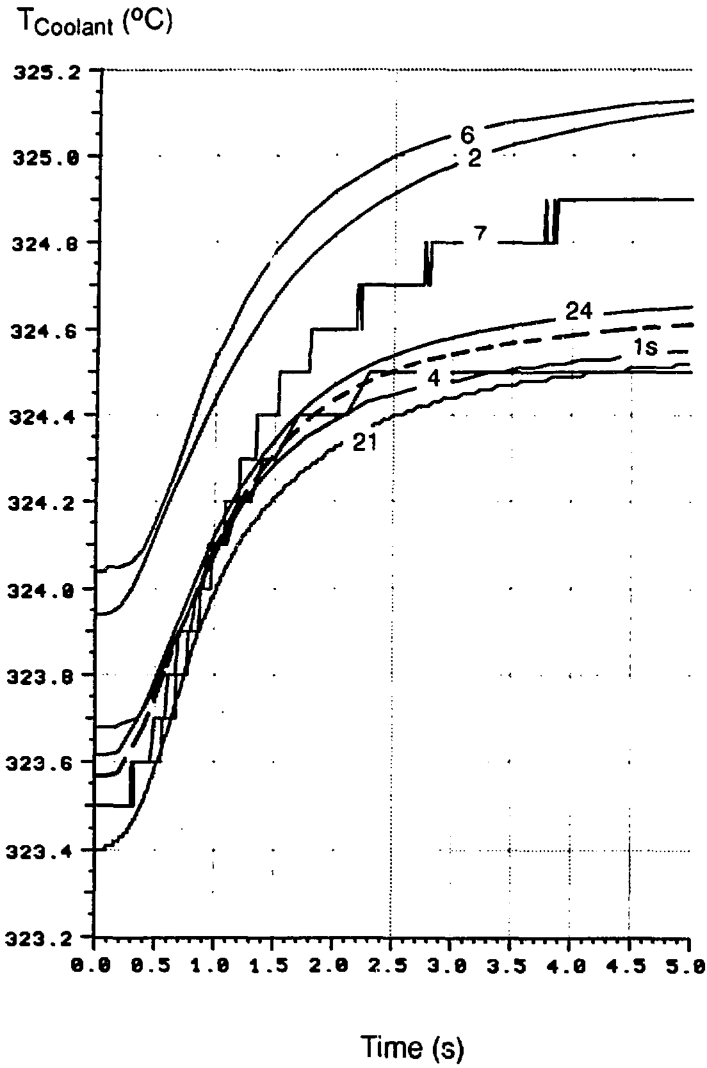

Fig. 4.1 PWR, CASE B1, Total Reactor Power versus Time

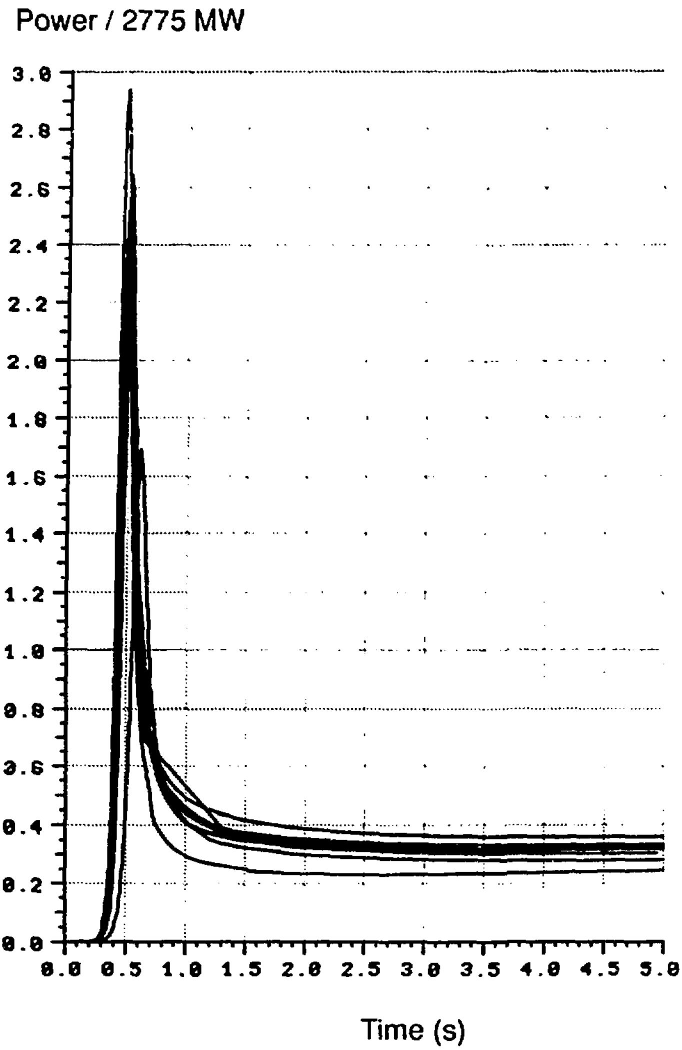

Fig. 4.2 PWR, CASE B1, Total Reactor Power versus Time

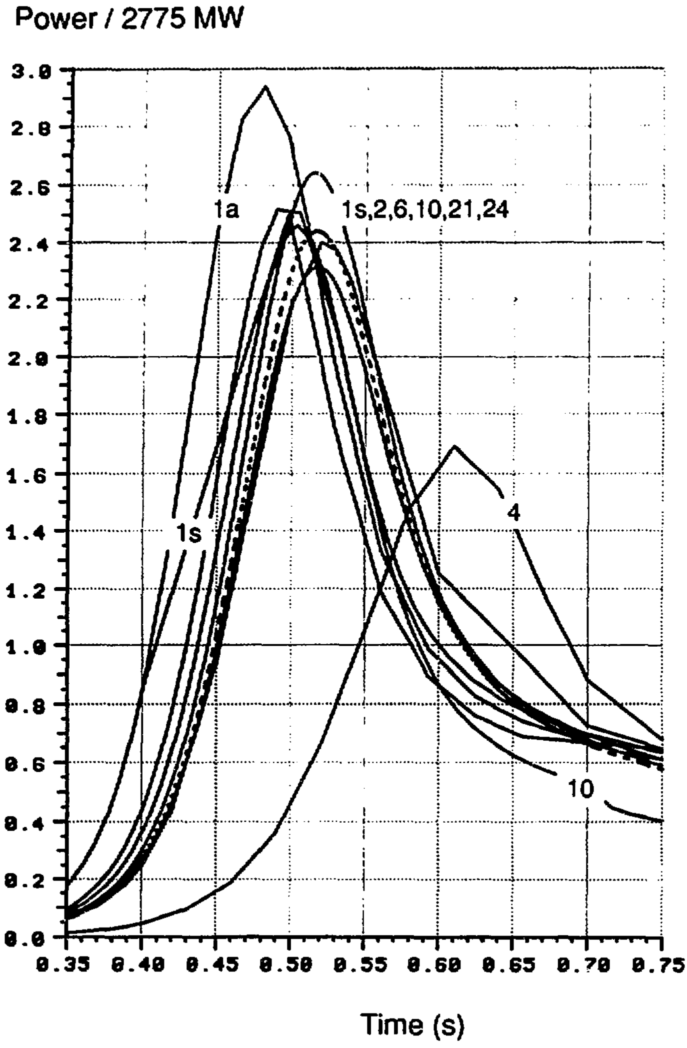

Fig. 4.3 PWR, CASE B1, Doppler Temperature versus Time

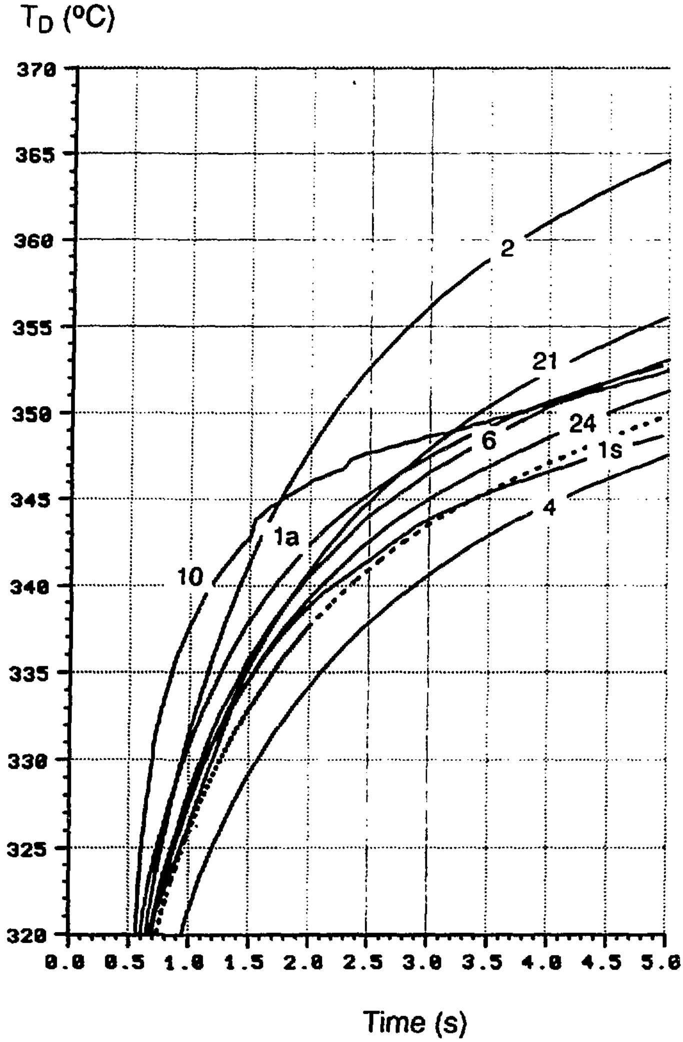

Fig. 4.4 PWR, CASE B1, Maximum Nodal Fuel Centerline Temperature versus Time

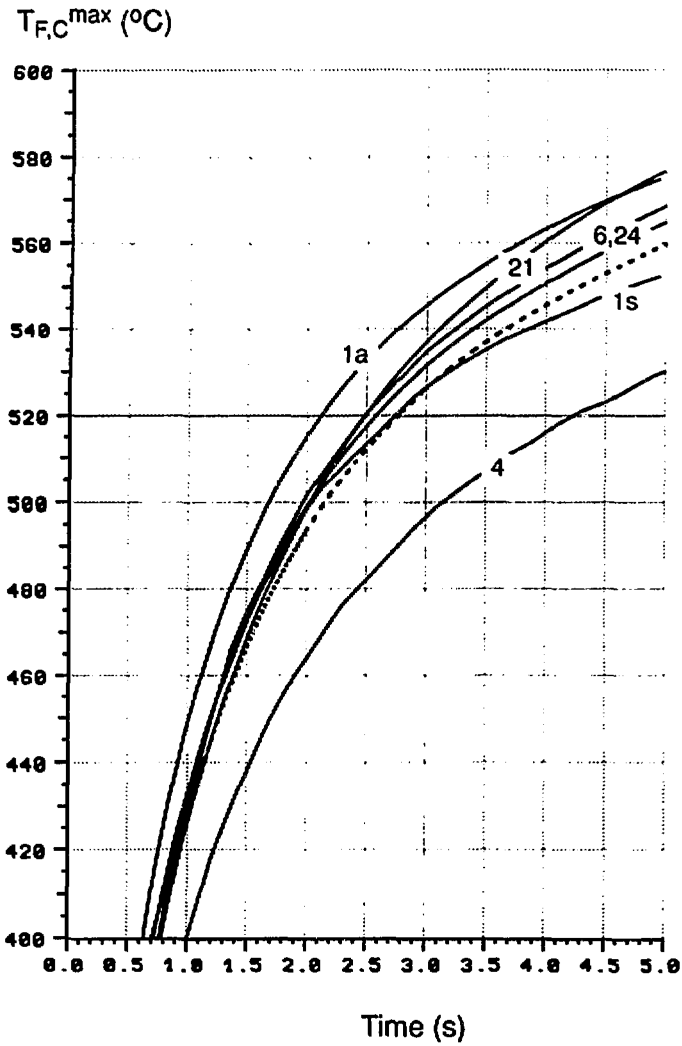

Fig. 4.5 PWR, CASE B1, Maximum Node Averaged Fuel Temperature versus Time

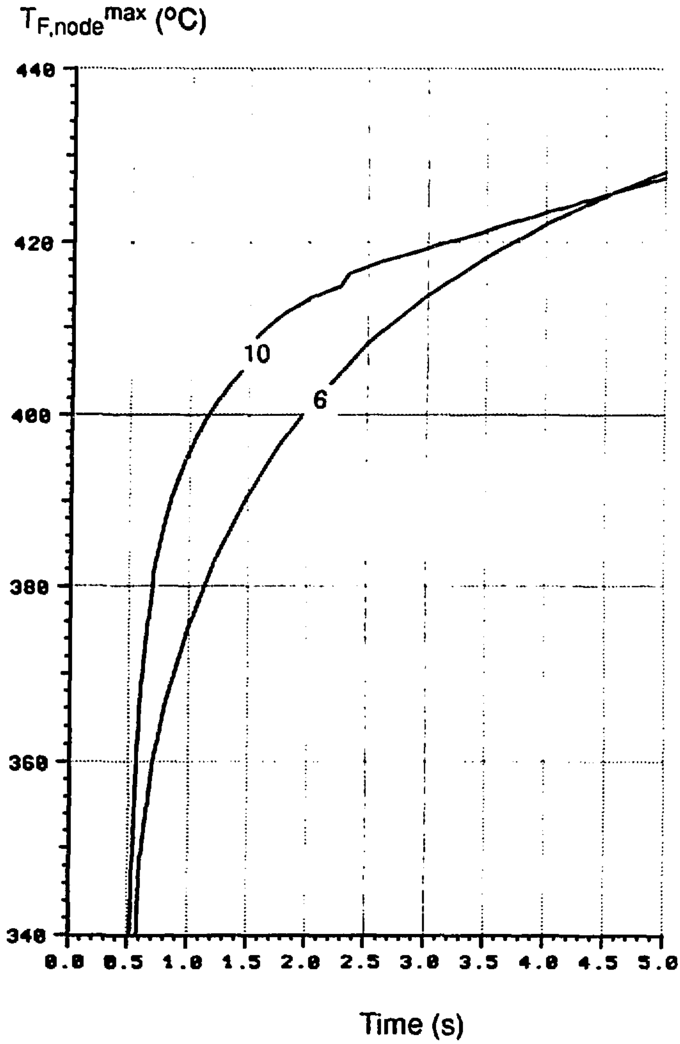

Fig. 4.6 PWR, CASE B1, Coolant Exit Temperature versus Time

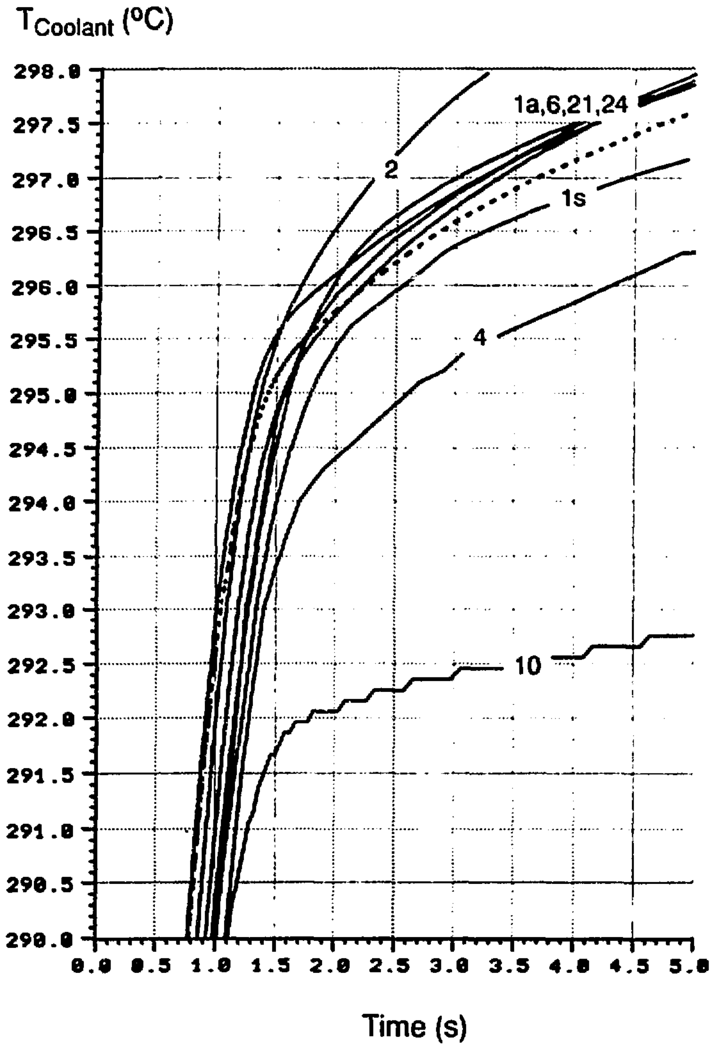

Fig. 5.1 PWR, CASE B2, Total Reactor Power versus Time

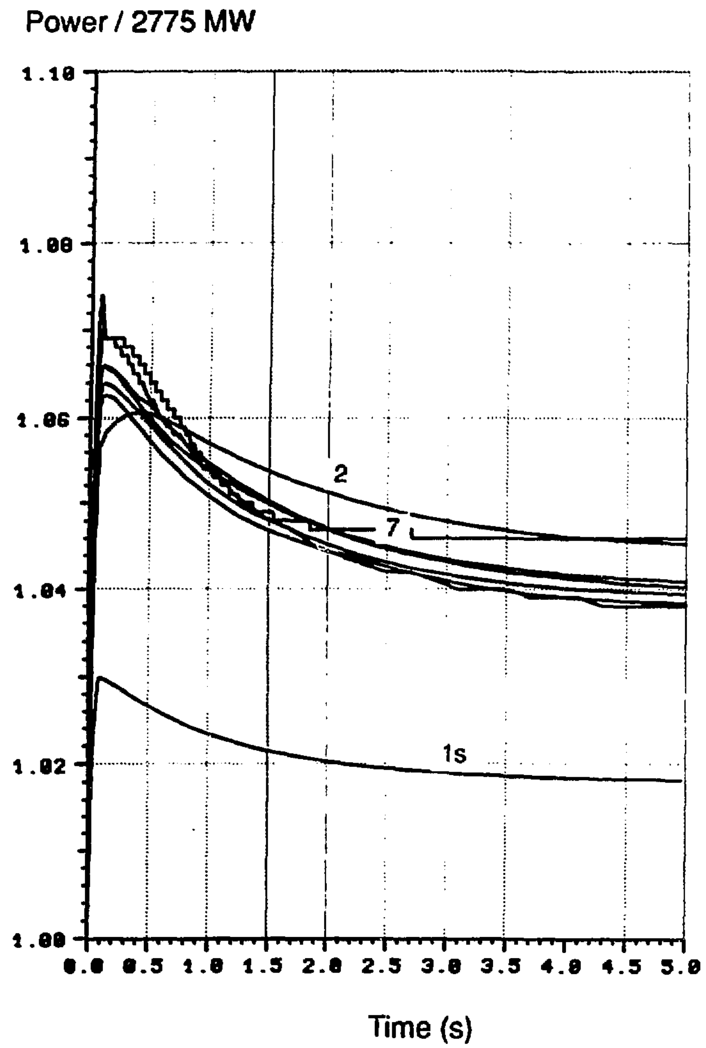

Fig. 5.2 PWR, CASE B2, Total Reactor Power versus Time

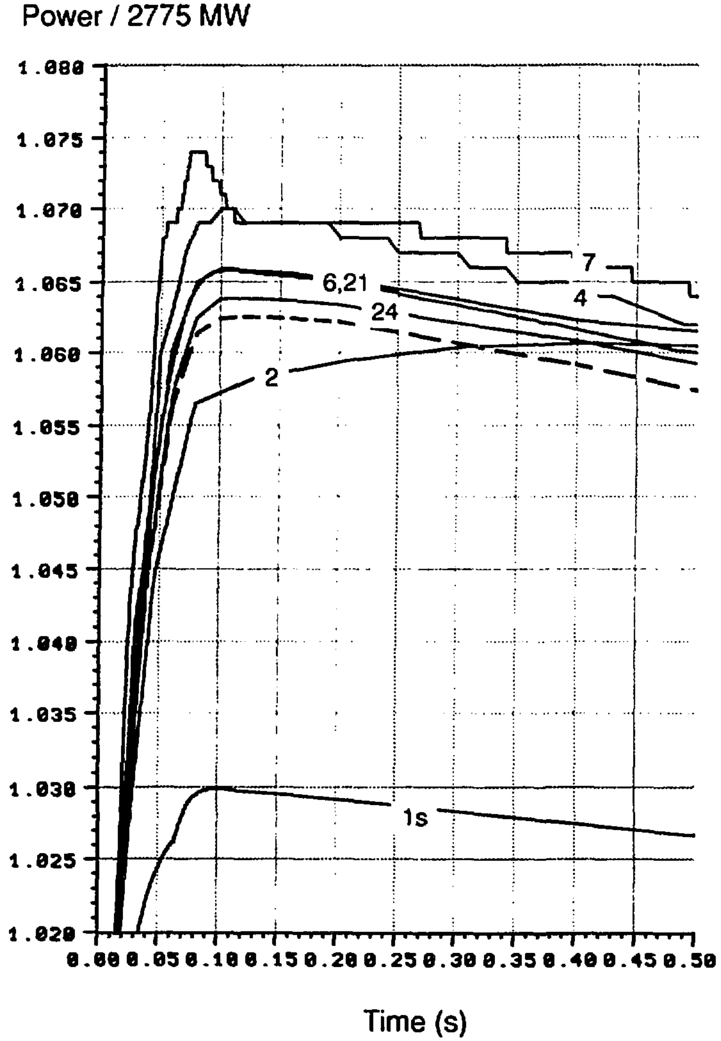

Fig. 5.3 PWR, CASE B2, Doppler Temperature versus Time

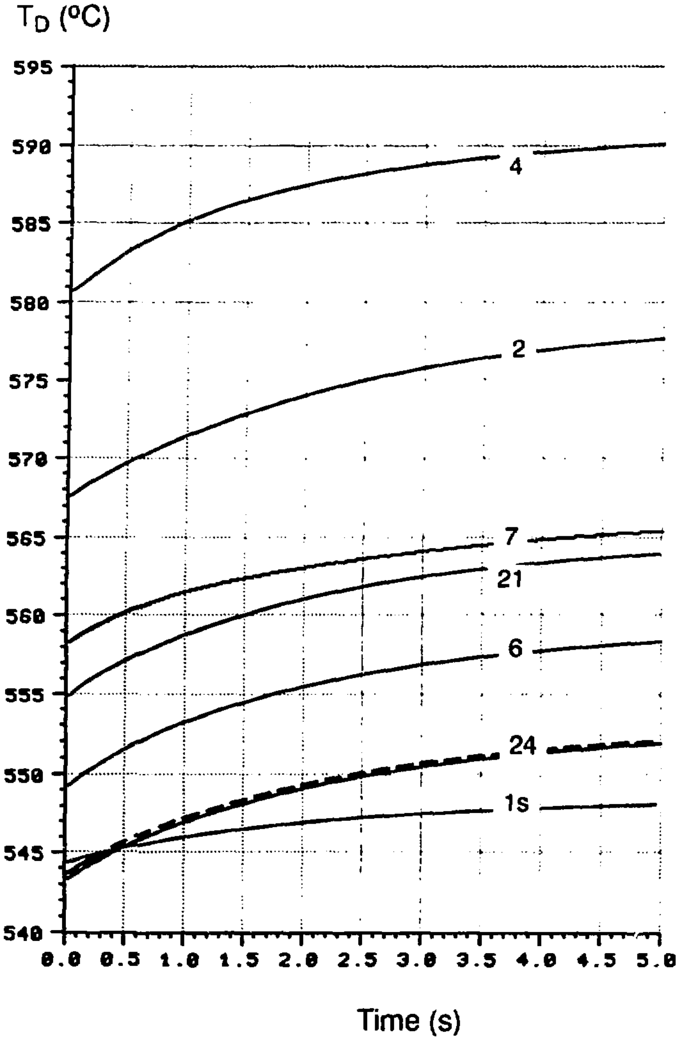

Fig. 5.4 PWR, CASE B2, Maximum Nodal Fuel Centerline Temperature versus Time

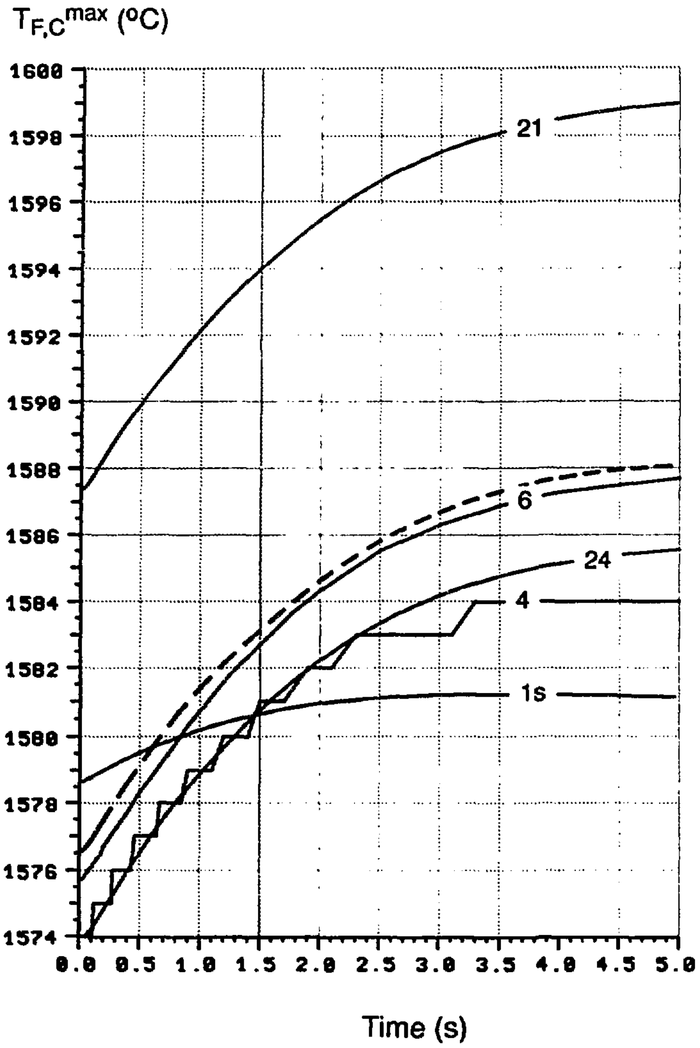

Fig. 5.5 PWR, CASE B2, Maximum Node Averaged Fuel Temperature versus Time

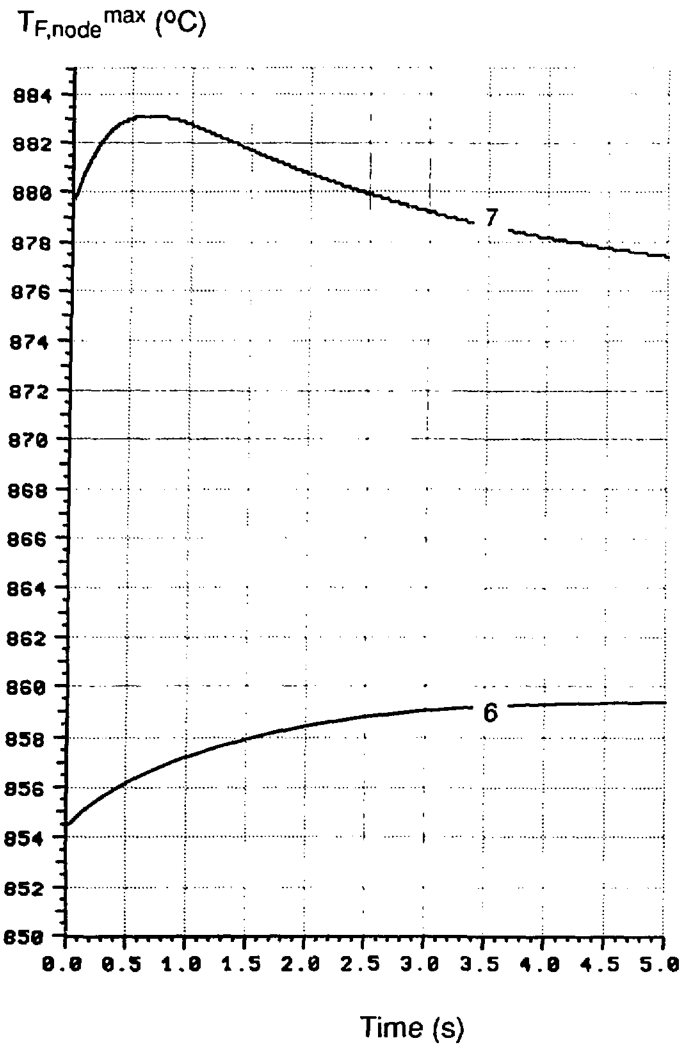

Fig. 5.6 PWR, CASE B2, Coolant Exit Temperature versus Time

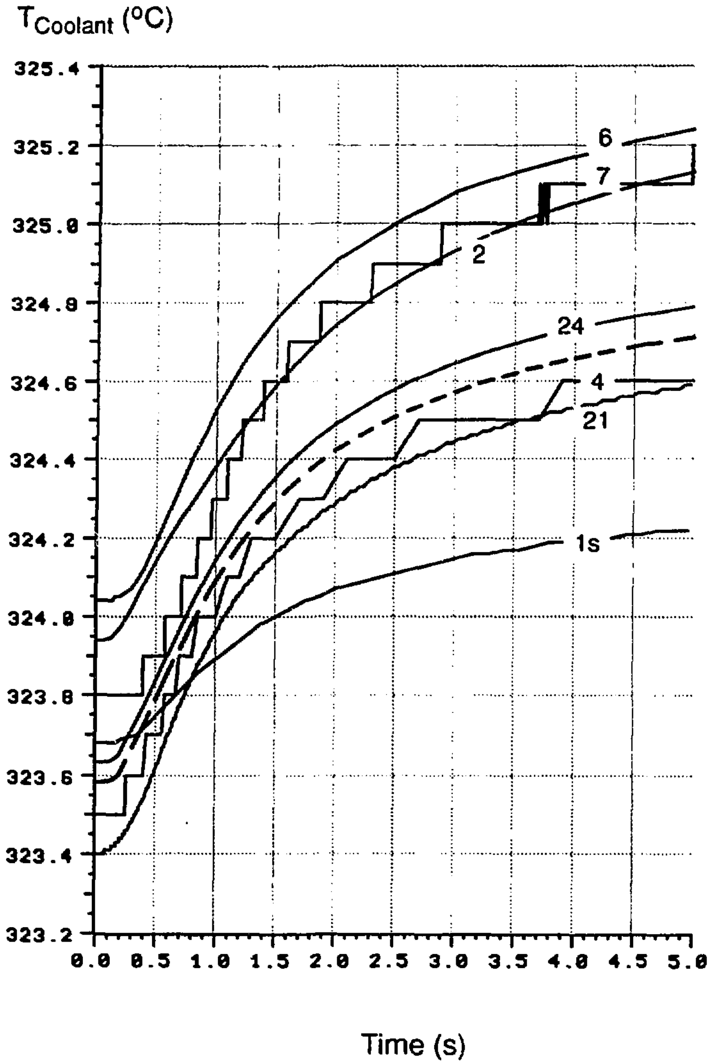

Fig. 6.1 PWR, CASE C1, Total Reactor Power versus Time

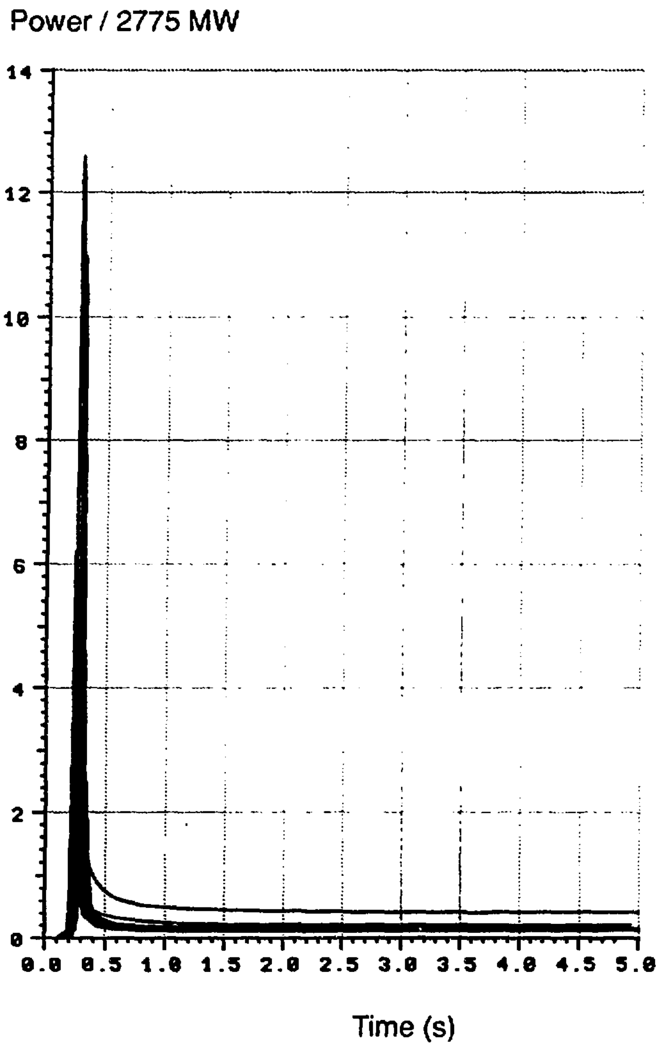

Fig. 6.2 PWR, CASE C1, Total Reactor Power versus Time

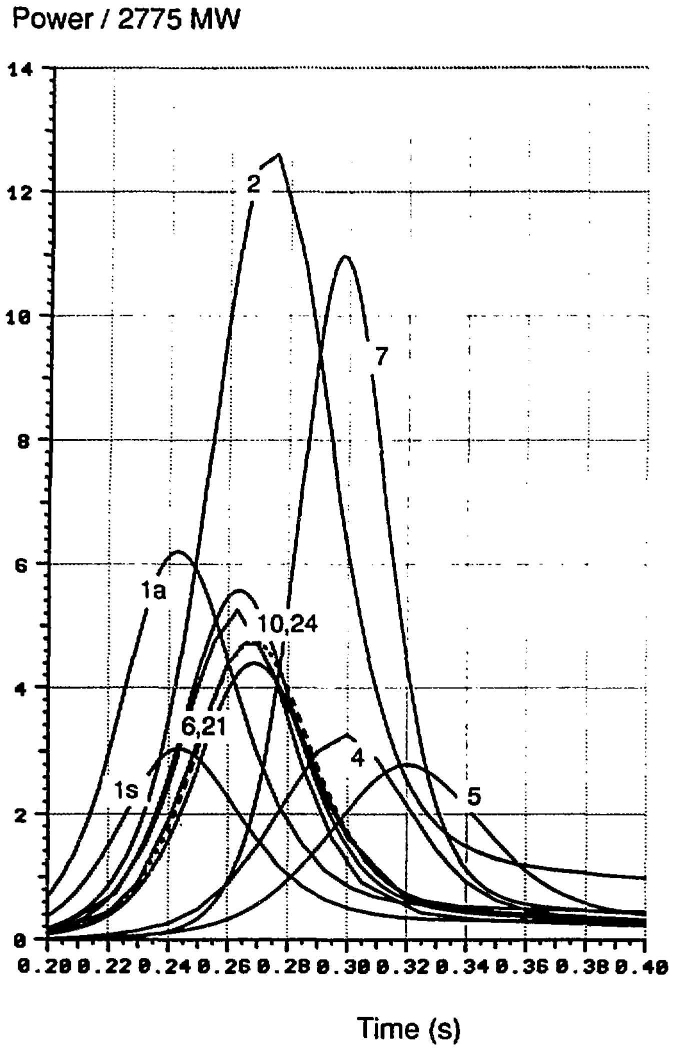

Fig. 6.3 PWR, CASE C1, Doppler Temperature versus Time

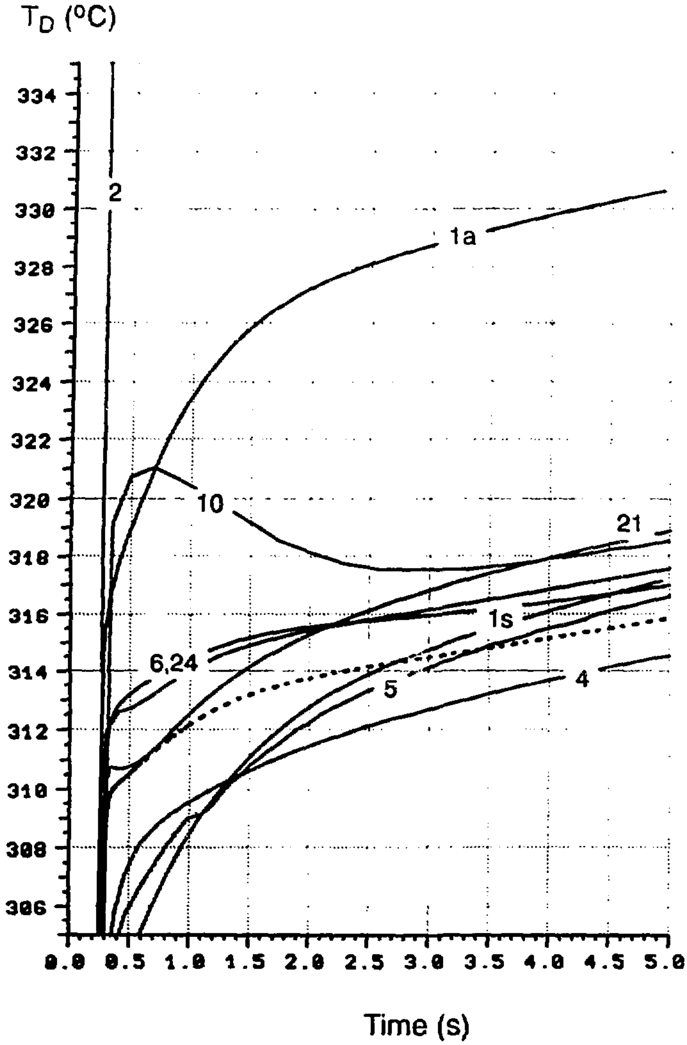

Fig. 6.4 PWR, CASE C1, Maximum Nodal Fuel Centerline Temperature versus Time

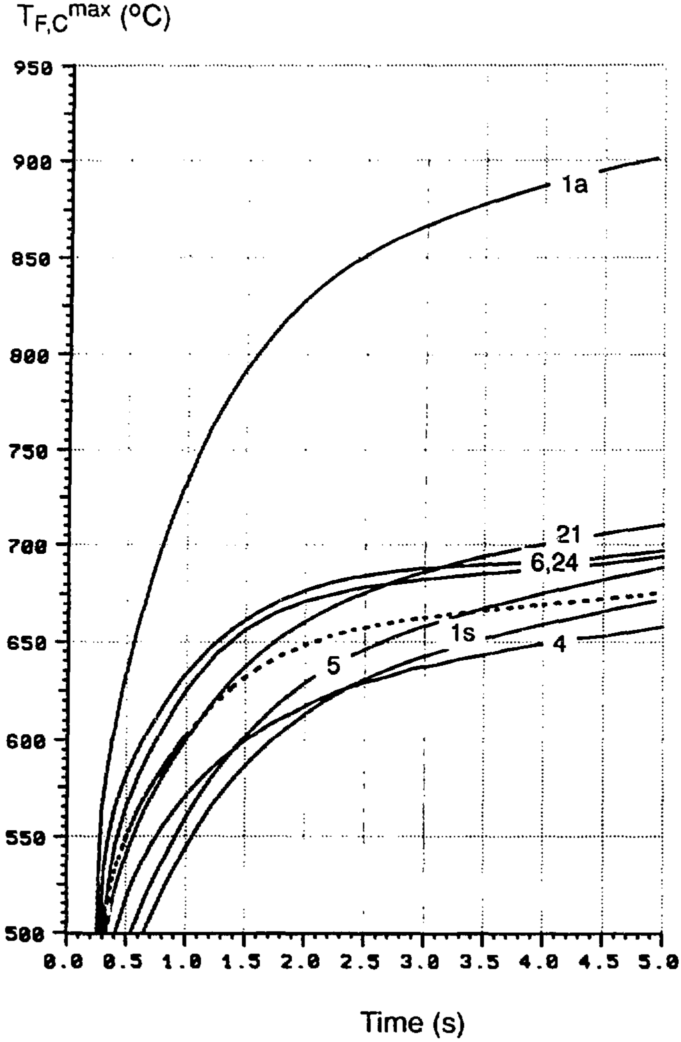

Fig. 6.5 PWR, CASE C1, Maximum Node Averaged Fuel Temperature versus Time

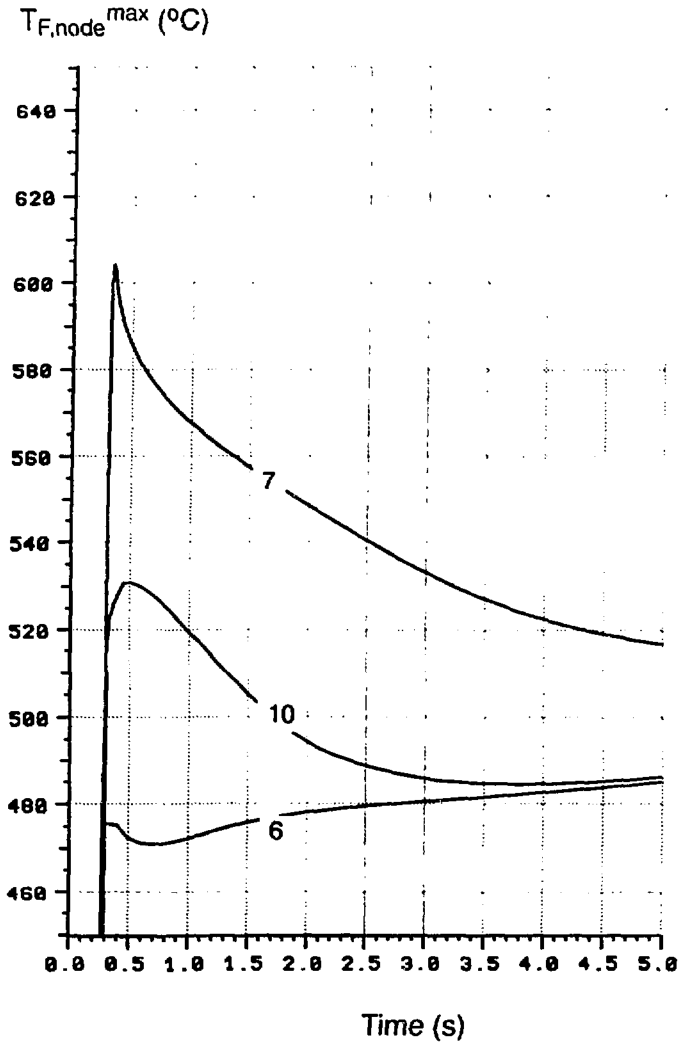

Fig. 6.6 PWR, CASE C1, Coolant Exit Temperature versus Time

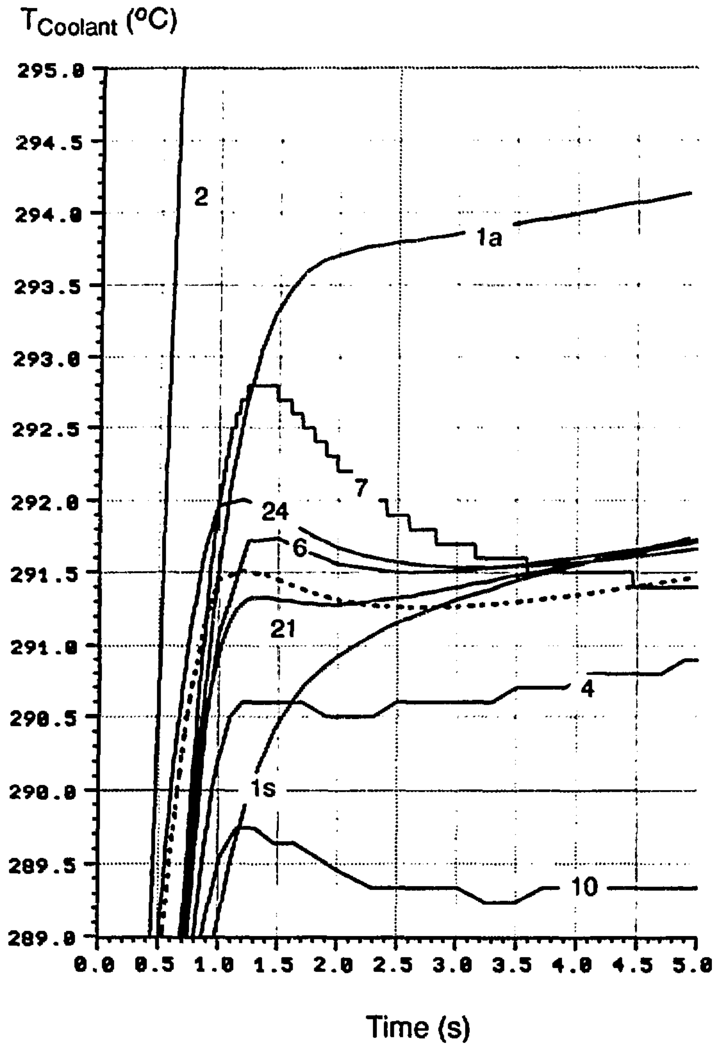

Fig. 7.1 PWR, CASE C2, Total Reactor Power versus Time

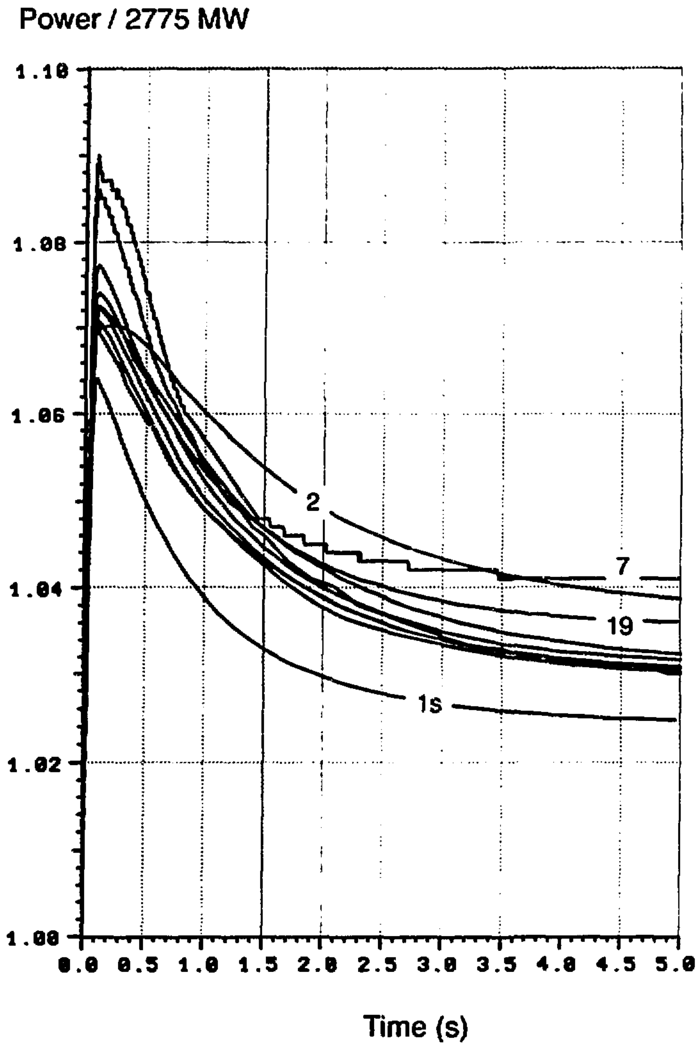

Fig. 7.2 PWR, CASE C2, Total Reactor Power versus Time

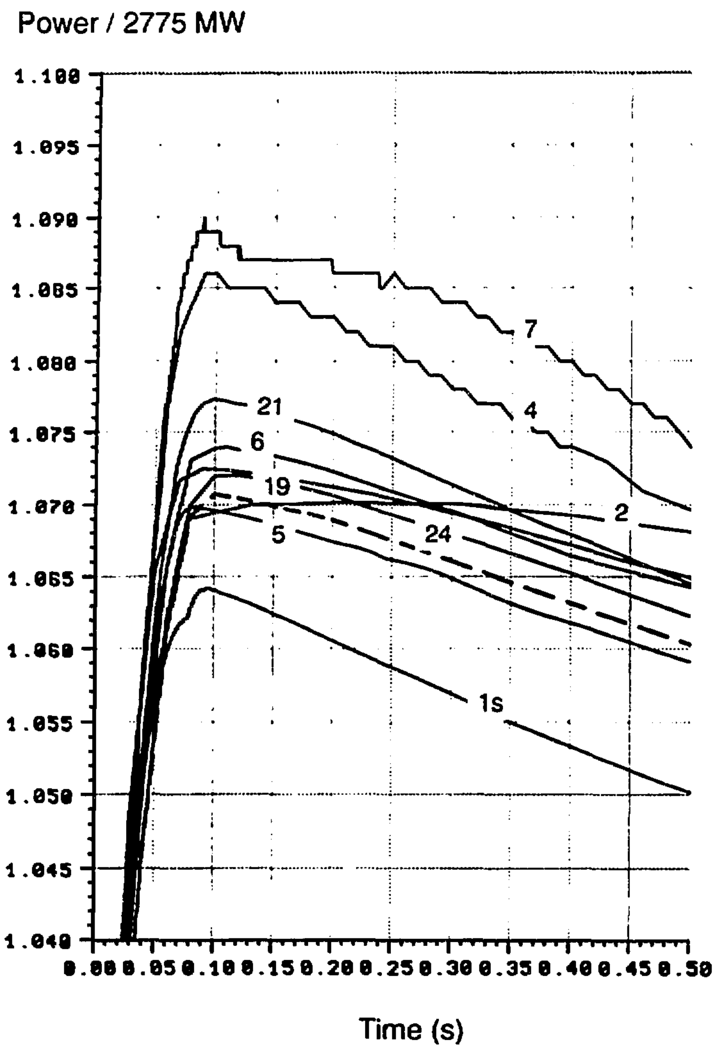

Fig. 7.3 PWR, CASE C2, Doppler Temperature versus Time

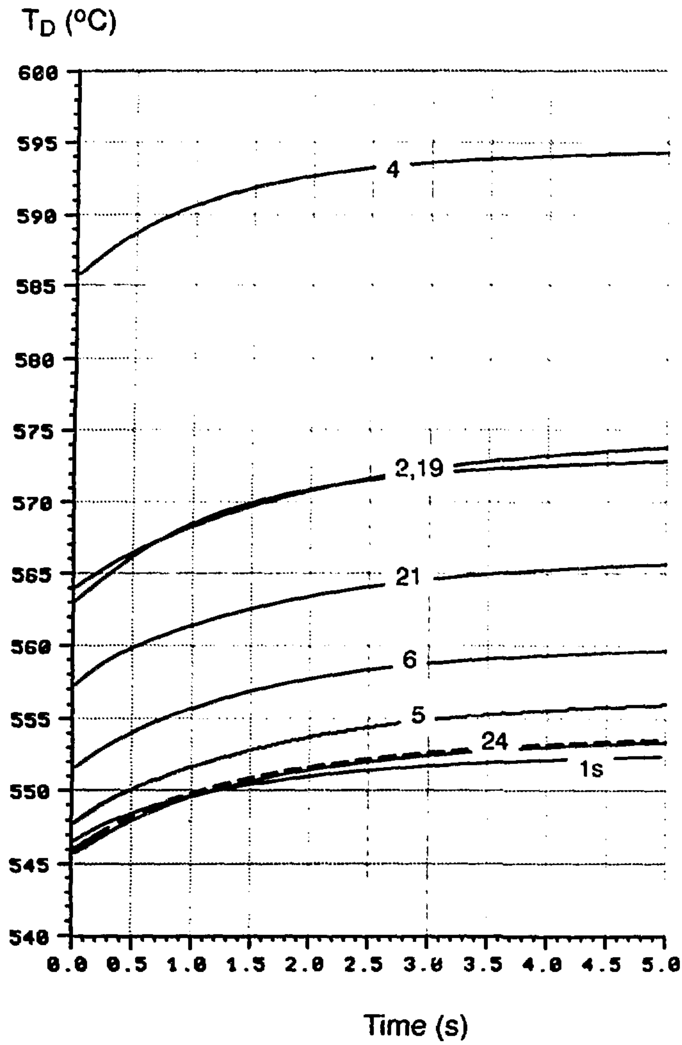

Fig. 7.4 PWR, CASE C2, Maximum Nodal Fuel Centerline Temperature versus Time

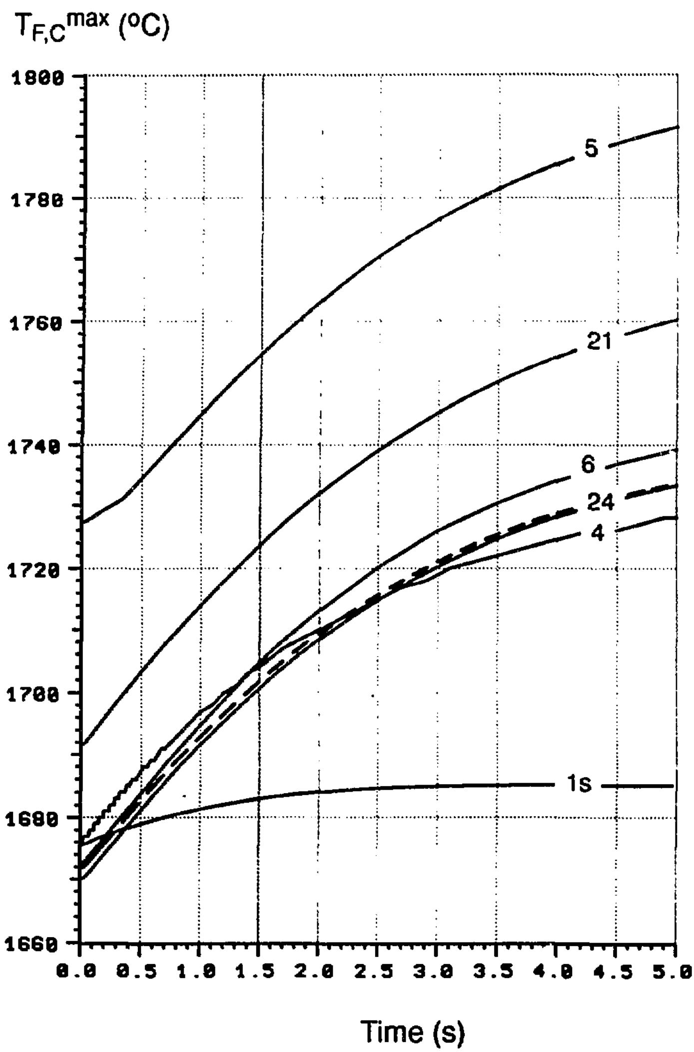

Fig. 7.5 PWR, CASE C2, Maximum Node Averaged Fuel Temperature versus Time

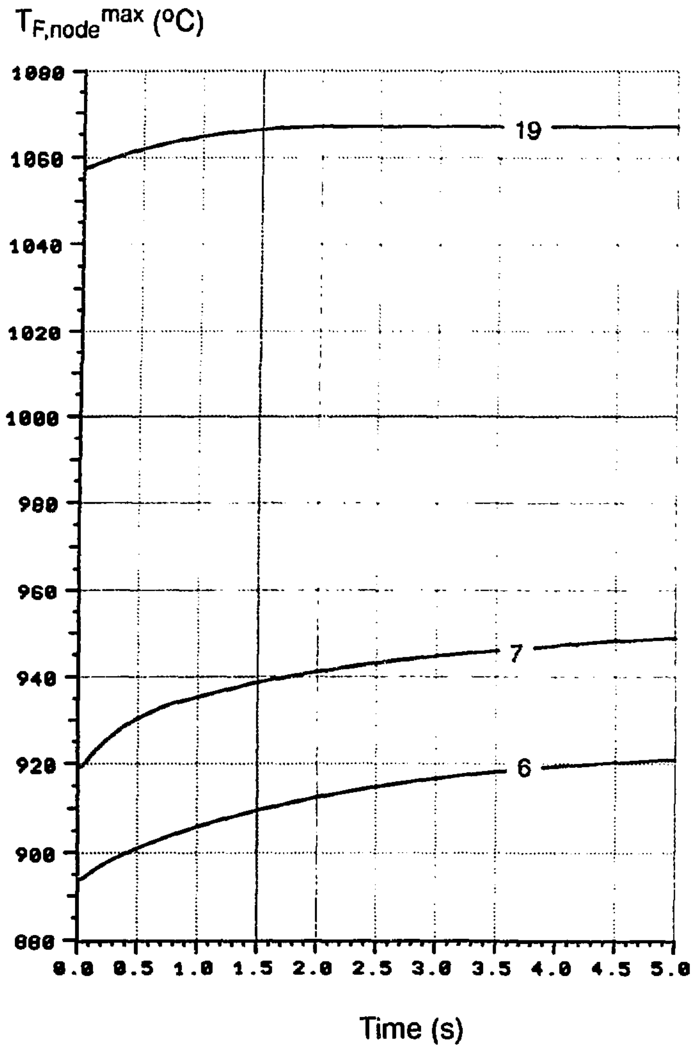

Fig. 7.6 PWR, CASE C2, Coolant Exit Temperature versus Time

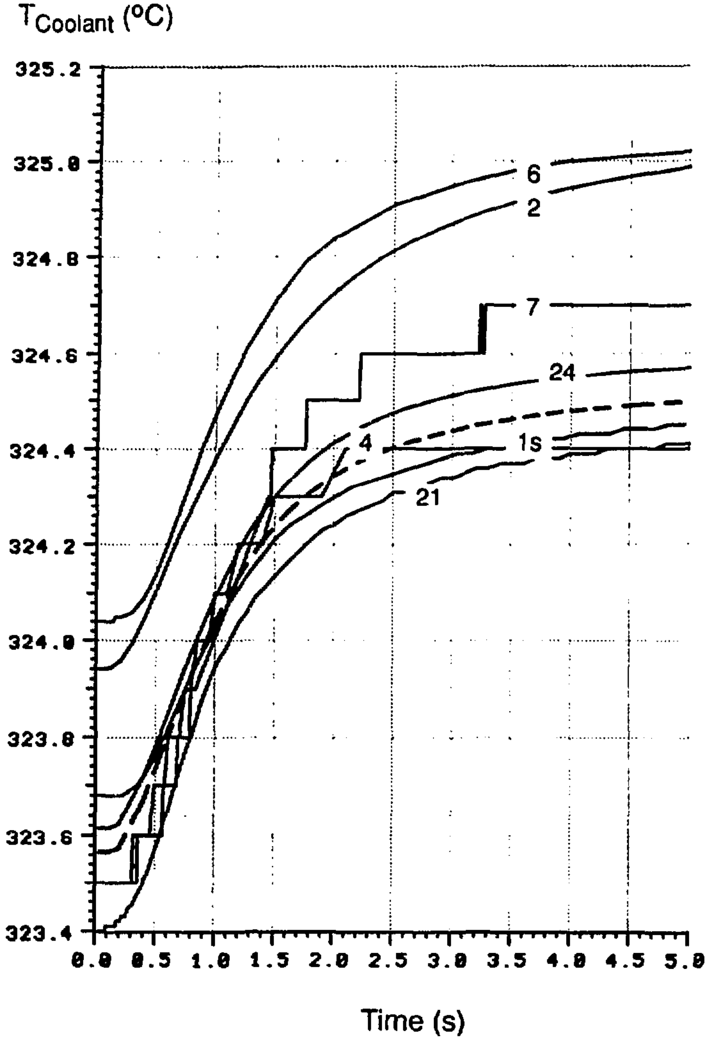

BWR, Key to Figures 8.1–8.7

ARROTTA

DYNAS

TNK-XC

KICOM

BOREAS

QUANDRY-EN

STAND

QUABOX-CUBBOX

Fig. 8.1 BWR, CASE D1: Steady–State Mass Flow Rate along the Vertical Traverse

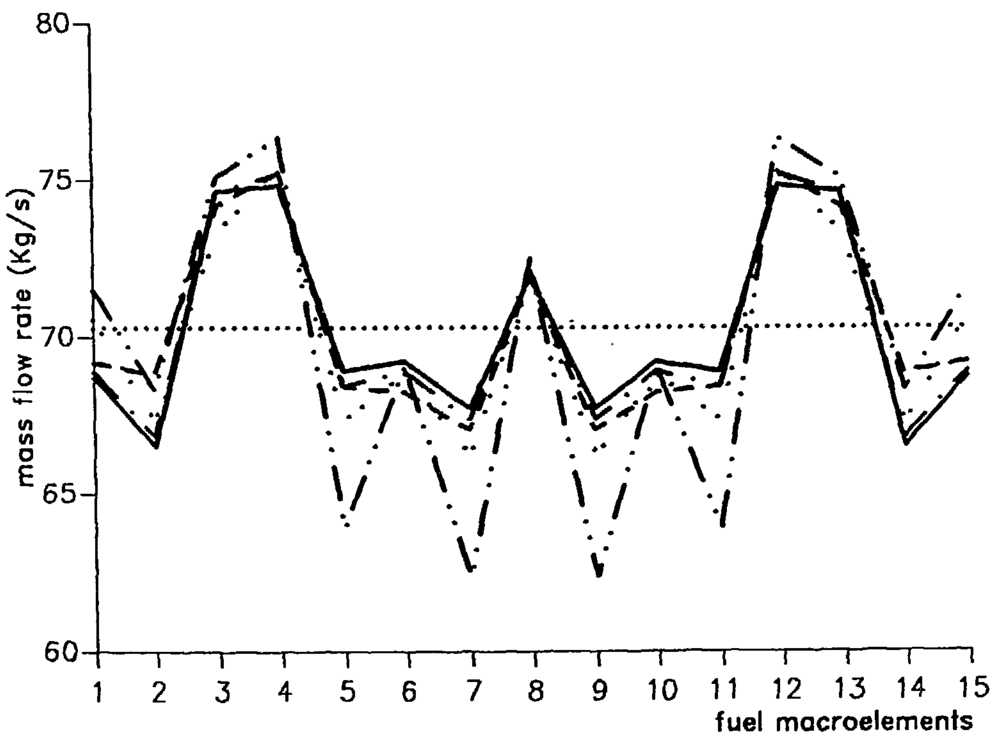

Fig. 8.2 BWR, CASE D1: Steady–State Normalized Axial Power

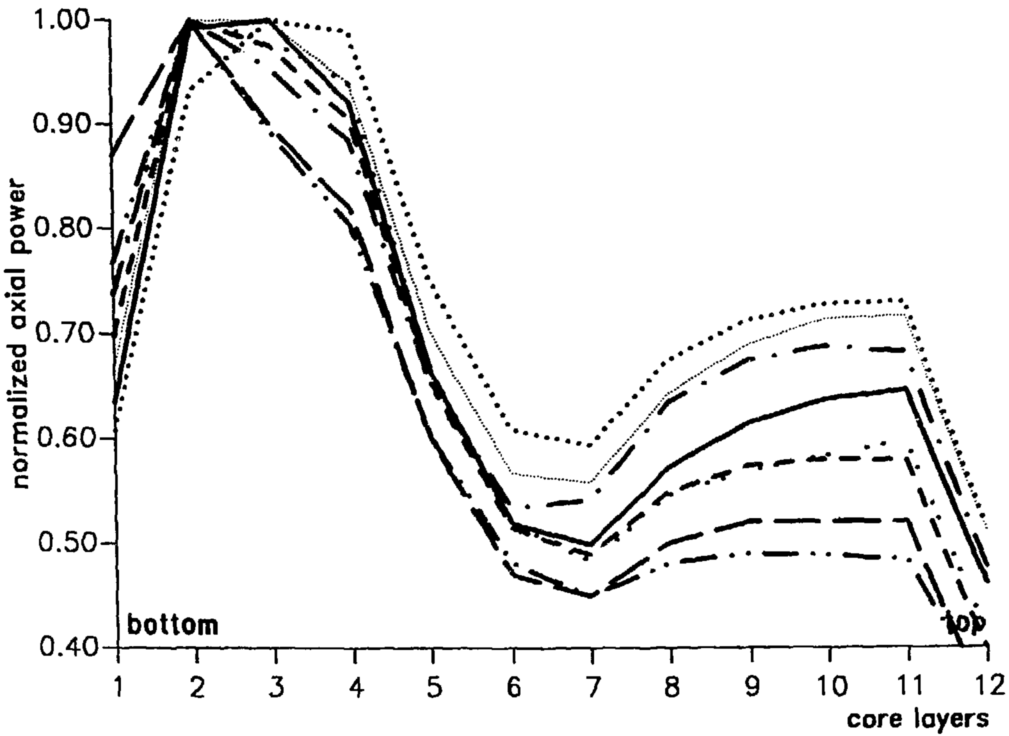

Fig. 8.3 BWR, CASE D1: Steady–State Outlet Density along the Vertical Traverse

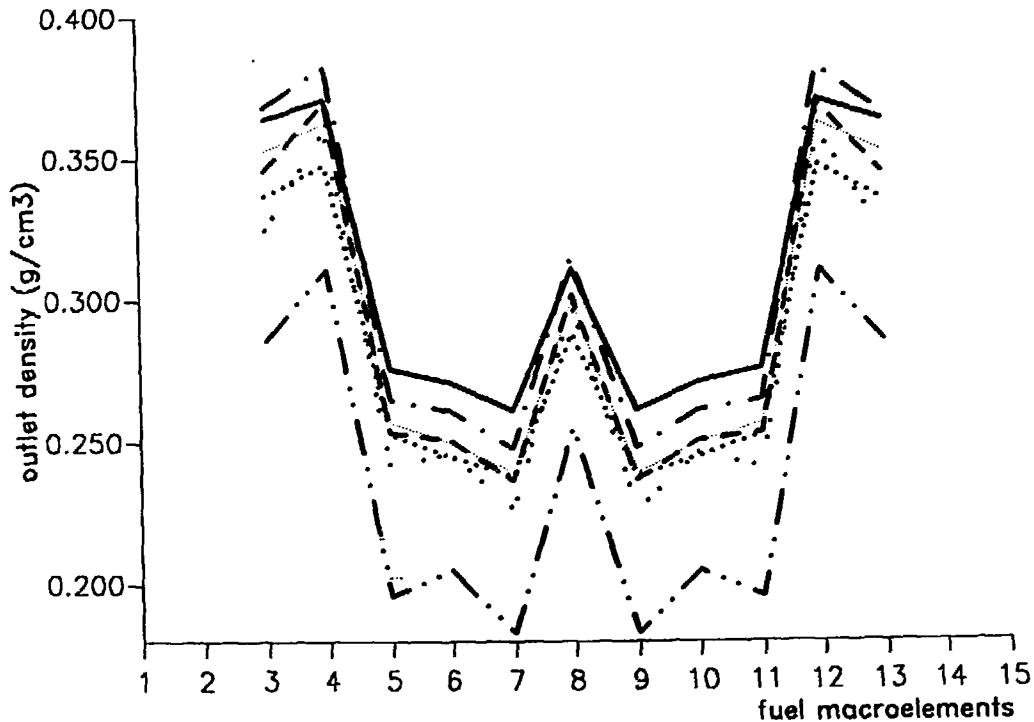

Fig. 8.4 BWR, CASE D1: Relative Power versus Time

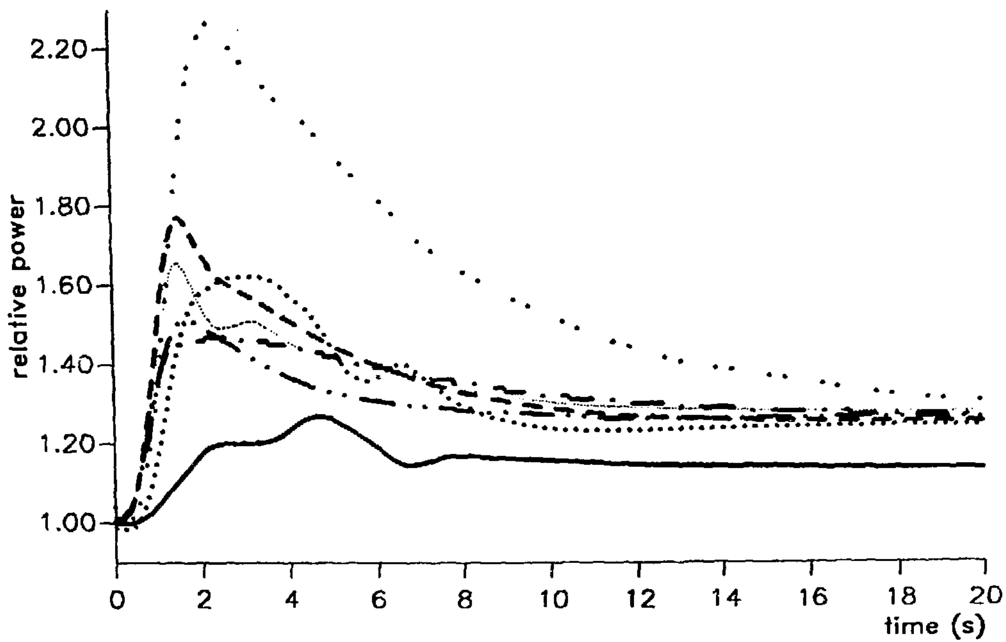

Fig. 8.5 BWR, CASE D1: Outlet Density Difference with Respect to Steady-State

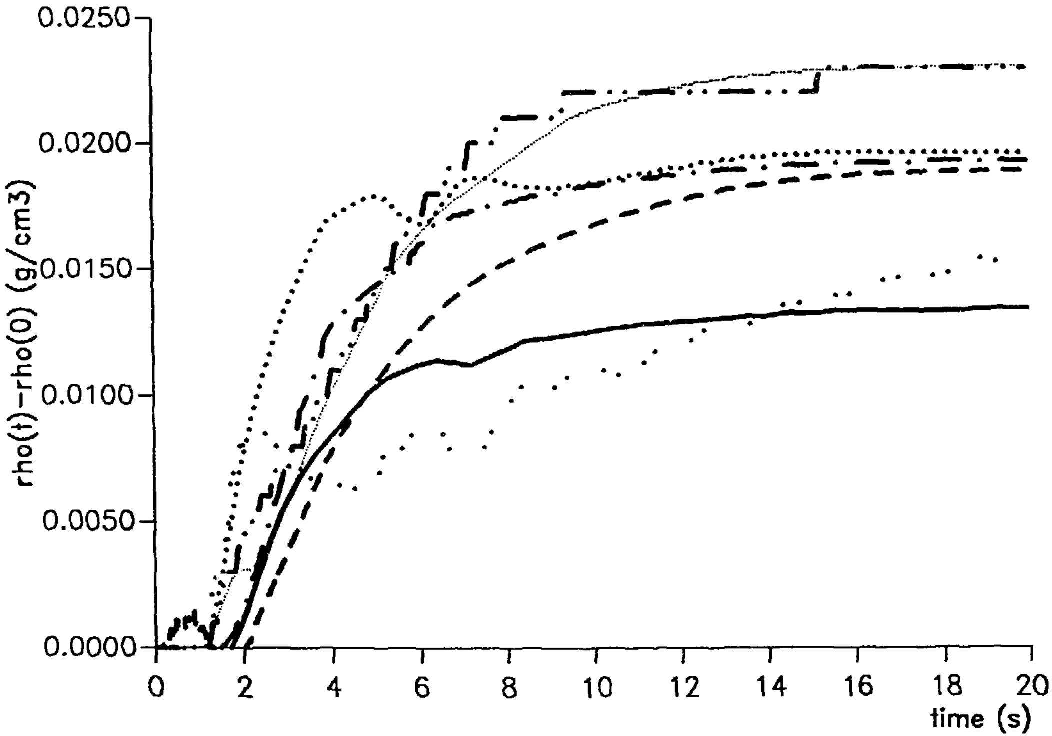

Fig. 8.6 BWR, CASE D1: Core Averaged Fuel Temperature Difference with Respect to Steady-State